The Discontinuous Flat Top Tent Map and the Nested Period Incrementing Bifurcation Structure

Ben Futter[1,*], Viktor Avrutin[1], Michael Schanz[1]

IPVS, University of Stuttgart, 70569 Stuttgart, Germany

Abstract

In this work we report the recently discovered nested period incrementing bifurcation scenario. The investigated piecewise linear map is defined on three partitions of the unit interval, constant in the middle partition and therefore displays a rich variety of superstable orbits. These orbits are arranged according to an infinite binary tree of the corresponding symbolic sequences, which can be generated by a simple set of rules. The system also allows for straightforward computation of the respective regions of existence. One of the most striking results of our investigations is that the famous U-sequence is inevitably embedded in the nested period incrementing scenario.

Keywords: discontinuous flat top tent map, nested period incrementing, symbolic dynamics, U-sequence, discontinuous maps

1. Introduction

Piecewise-smooth dynamical systems are in the meanwhile well-known to be important as adequate models of many technical applications. Among these applications appearing from several fields there is a class of systems with the common property that the system function is constant on some partition in the state space. One example is limiter control of unimodal maps [1, 2, 3, 4, 5], which is applicable for chaos control [6] or the control of cardiac arrhythmia [7, 8]. In a special case, a simplified model of front propagation in semiconductor superlattices [9] also yields a related, piecewise-linear map defined on three partitions with one flat interval. Further examples can be found in the field of electronic converters [10, 11]. It is worth noticing that such systems show a broad spectrum of complex bifurcation structures which were observed experimentally but barely investigated. To our knowledge, the earliest mentioned dynamical system belonging to the class of piecewise smooth maps with a constant value on one of the partitions is the *flat top tent map* introduced in the famous work by Metropolis, Stein and Stein [12]. In this work, the authors demonstrated that the stable periodic orbits of this map are organized in the same manner as the orbits of the logistic map, that means according to the *universal sequence*, also known as U-sequence or Metropolis-Stein-Stein sequence.

Recall that, recently, *discontinuous* piecewise smooth systems attracted more and more attention of the researchers from several fields. Therefore, one may ask the following question: what happens, if one modifies the flat top tent map in such a way that it becomes discontinuous? This seemingly unmotivated question turns out to be of interest. As we will see, the discontinuous flat top tent map we consider in this paper demonstrates a bifurcation scenario which has already been observed in an electronic circuit, as reported in

*Corresponding author

Email addresses: Ben.Futter@ipvs.uni-stuttgart.de (Ben Futter), Viktor.Avrutin@ipvs.uni-stuttgart.de (Viktor Avrutin), Michael.Schanz@ipvs.uni-stuttgart.de (Michael Schanz)

Published in 'Chaos, Solitons & Fractals', April 2012, Vol. 45(4), pp. 465-482

http://dx.doi.org/10.1016/j.chaos.2012.01.009

[10]. However, this scenario was investigated neither in [10], nor in any other work so far. This is (among other reasons) due to the fact that, in the system considered in the cited work, this scenario is mixed with other phenomena, which makes the investigation more complicated. By contrast, in our map this scenario occurs in its pure form and can also be completely explained by analytical arguments. This explanation is the main objective of this paper.

The paper is organized as follows. In §2 we introduce the discontinuous flat top tent map and identify the region in its parameter space which is relevant for our work (§2.1). Next we discuss the bifurcation structure to be explained (§2.2) and the mechanisms leading periodic orbits to occur in this system (§2.3). As a next step in §3 we investigate the considered bifurcation scenario at a particular parameter value where it appears in its fully developed form. We explain the bifurcation structure by proving that in this case it is formed by stable periodic orbits corresponding to all possible symbolic sequences (§3.1). Additionally, we show that unstable orbits may become Milnor attractors (§3.2). In §4 we extend our results for other parameter values where the bifurcation scenario we investigate occurs in a truncated form. For any given parameter value we explain why not every periodic orbit can exist (§4.1) and give a constructive approach which allows to determine the subset of stable periodic orbits existing at a given parameter value (§4.2). In §4.3 we reconsider and explain the examples discussed in §2.2. Additionally, in §5 we show the connection of the bifurcation structure we investigate with the U-sequence (§5.1). We demonstrate that the results obtained for the discontinuous flat top tent map are also useful for explanation of the bifurcation scenarios in other maps defined on three partitions (§5.2) and that they allow us also to generate bifurcation scenarios where the periods determined according to the U-sequence are modified by some (positive or negative) offset (§5.3).

2. System Properties

Let us consider the piecewise linear map, defined by

$$x_{n+1} = f(x_n) \quad \text{with} \quad f(x) = \begin{cases} f_{\mathcal{L}}(x) = 2\alpha x & \text{if} \quad x \leq \frac{1-\gamma}{2} \\ f_{\mathcal{C}}(x) = \beta & \text{if} \quad \frac{1-\gamma}{2} < x < \frac{1+\gamma}{2} \\ f_{\mathcal{R}}(x) = 2\alpha(1-x) & \text{if} \quad x \geq \frac{1+\gamma}{2} \end{cases} \tag{1}$$

as shown in Fig. 1. The parameters α, β and γ denote the tent tip height, the height and the width of the constant interval, respectively.

This map can be considered as an extension of the flat top tent map with an additional parameter β, which leads the map to be discontinuous in general. The system (1) is therefore referred to as *discontinuous flat top tent map* in the following. This system turns out to demonstrate a number of interesting properties concerning its stable and unstable periodic orbits and — as we will see later — is helpful for the understanding of the dynamics of other piecewise-smooth maps, especially those defined on three partitions.

Note that a similar extension of the flat top tent map was already considered in [13]. However, in this work the value of the function on the middle partition was set to a value outside the interval $[0, 1]$, so that every orbit reaching this partition diverges. By contrast, we consider the values on this partition (given by the parameter β) which do not lead to divergence.

Note that as the functions $f_{\mathcal{L}}$, $f_{\mathcal{C}}$ and $f_{\mathcal{R}}$ are linear, the map can have at most three fixed points

$$x_{\mathcal{L}} = 0, \qquad x_{\mathcal{C}} = \beta, \qquad x_{\mathcal{R}} = \frac{2\alpha}{2\alpha + 1}. \tag{2}$$

The fixed point $x_{\mathcal{L}}$ exists for all parameter values, whereas $x_{\mathcal{C}}$ and $x_{\mathcal{R}}$ may exist or not depending on the particular parameter values.

2.1. Parameter Space

Let us first identify the region in the parameter space which will be investigated in the following. In order to be in a similar situation as with the usual flat top tent map, we assume $\alpha \geq 0$. Naturally, we also take γ to be non-negative, as it represents the width of an interval.

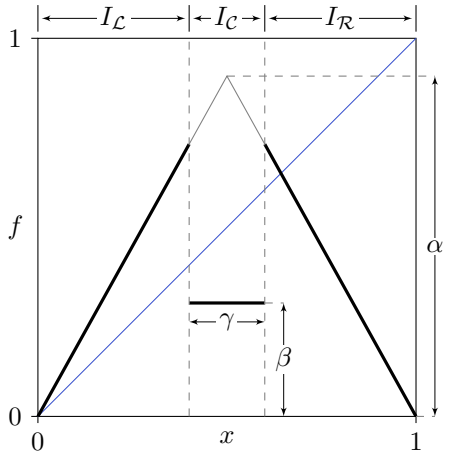

Figure 1: Discontinuous flat top tent map (1) and symbolic labeling of its partitions.

For $\gamma = 0$ we get the usual tent map, whereas for $\beta \in [0,1]$ (the case we consider in the following) and $\gamma = 1$ all initial values from the interval $(0,1)$ are directly mapped to the fixed point $x_\mathcal{C}$. The orbits started outside the interval $(0,1)$ are attracted by the fixed point $x_\mathcal{L}$ for[1] $\alpha \in \left[0, \frac{1}{2}\right)$ or diverge for $\alpha > \frac{1}{2}$. It turns out that between these two limiting cases the role of the parameter γ is negligible. In fact, there is no affine transformation which allows to get rid of this parameter, but the variation of γ does not lead to any topological changes of the complete bifurcation structure in the (α, β) parameter plane. Therefore, unless stated otherwise, we use the value $\gamma = 0.1$ in all numerically calculated figures, for the sake of consistency. As will turn out later, the analytical arguments remain equivalent independently of the particular choice of $\gamma \in (0,1)$.

For $\alpha < \frac{1}{2}$, the fixed point $x_\mathcal{L}$ is asymptotically stable. At $\alpha = \frac{1}{2}$, the system undergoes a degenerate bifurcation associated with the eigenvalue $+1$ [14] and each point $x \leq \frac{1-\gamma}{2}$ is a fixed point. For $\alpha > \frac{1}{2}$, $x_\mathcal{L}$ is unstable.

With the origin unstable, we rule out the cases $\beta < 0$ and $\beta > 1$, investigated in [13]. For both cases, orbits which enter the middle interval will be mapped to the left of the origin after one or two iterations, respectively and diverge to $-\infty$. Orbits which *don't* enter the middle interval are unstable anyway, as will be shown later in Theorem 1. Accordingly, we assume $\beta \in [0,1]$ in the following. It is worth noticing that also in this region diverging orbits may exist. This is possible if there exists a point x with $f(x) > 1$, for which we need to choose α such that

$$\max_{x \in [0,\, x^r_\mathcal{L}]} f(x) = 2\alpha x^r_\mathcal{L} = \alpha\,(1-\gamma) \;>\; 1 \tag{3}$$

where $x^r_\mathcal{L} = \frac{1-\gamma}{2}$ is the right border of the left partition. Due to the symmetry of the system function with respect to $x = \frac{1}{2}$ the same condition can also be written using the value at the left border of the right partition. Clearly, the smallest value satisfying this condition is

$$\alpha^\star = \frac{1}{1-\gamma}. \tag{4}$$

Thus, diverging orbits are possible as well as periodic ones for $\alpha > \alpha^\star$. To sum up, we will investigate the behavior in the parameter plane (α, β) with

$$\alpha \in \left(\tfrac{1}{2}, \infty\right), \tag{5}$$

$$\beta \in \big[0,1\big] \quad \text{and} \quad \gamma = const \in \big(0,1\big). \tag{6}$$

[1] which is one-side attracting in this case, but not an attractor

It can easily be seen that within these parameter ranges, every orbit started at an initial value outside the interval $I = [0, 1]$ diverges. Therefore, we consider in the following the map f on the interval $[0, 1]$ where all bounded orbits are located. According to the definition of f, we introduce the following three sub-intervals (partitions):

$$I_{\mathcal{L}} = \left[0, \tfrac{1-\gamma}{2}\right], \quad I_{\mathcal{C}} = \left(\tfrac{1-\gamma}{2}, \tfrac{1+\gamma}{2}\right), \quad I_{\mathcal{R}} = \left[\tfrac{1+\gamma}{2}, 1\right]. \tag{7}$$

2.2. Bifurcation Scenarios

Fig. 2 shows four bifurcation scenarios calculated numerically for fixed α and varying β:

a) For $\alpha = 0.6$, we can see an interval where a fixed point exists and, to both sides of this interval, two symmetric period incrementing cascades, which accumulate at the boundaries of $\beta \in [0, 1]$.
b) For $\alpha = 0.75$, we see that the scenario as in a) is interrupted between any two adjacent periods, by a pair of period incrementing cascades. Both cascades have the increment value two and accumulate to a common point in between.
c) For $\alpha = 0.85$, the scenario as in b) is again interrupted, by a pair of opposite period incrementing cascades with the increment value four.
d) For $\alpha = 0.9$, the scenario is already much further developed, although not fully. However, the diagram hints at the overall complexity of the bifurcation structure.

Due to this series of cumulative period incrementing cascades, we refer to this scenario as *nested period incrementing*. It becomes apparent that the scenario becomes increasingly complex for higher values of α. To explain this increasing complexity, it is necessary to consider the bifurcation structure of the 2D parameter plane (α, β). This structure is presented in Fig. 3 and shows the bifurcation curves separating regions of different periods. The dashed lines indicate the location of the 1D bifurcation diagrams in Fig. 2. Furthermore, two critical values, α_1 and $\alpha^\star$ are pointed out. For $\alpha \geq \alpha_1$, where the value α_1 is defined by the condition $f_{\mathcal{R}}(\frac{1+\gamma}{2}) = \frac{1+\gamma}{2}$ and is given by

$$\alpha_1 = \frac{1+\gamma}{2(1-\gamma)}, \tag{8}$$

the system has an unstable fixed point in the partition $I_{\mathcal{R}}$ whereas for smaller values this is not the case. As a consequence, for $\alpha < \alpha_1$ there is only simple period incrementing as shown in Fig. 2a, whereas for $\alpha \geq \alpha_1$ the bifurcation structure becomes more complicated (see Figs. 2b and c).

For α increasing in the interval $\left[\alpha_1, \alpha^\star\right]$ we see that new regions appear successively, giving rise to the above mentioned increase in complexity. This process accumulates to the value $\alpha = \alpha^\star$. At this value all possible periodic orbits "are already created" so that no new orbits can emerge for $\alpha > \alpha^\star$. In some sense, the situation at $\alpha = \alpha^\star$ is similar to the situation of the logistic map $x_{n+1} = \mu x_n(1 - x_n)$ at $\mu = 4$. In both cases, all possible periodic orbits exist and the divergent behavior begins. For our system the former property will be proved in Sec. 2.3 by Theorem 2, whereas the latter was already shown above, see Eqs. (3,4). In Fig. 3 the regions of divergent behavior are colored blue. Moreover, for $\alpha \to \infty$ we see that all non-diverging orbits accumulate at $\beta = 0$ and $\beta = 1$.

The observations presented above lead us to proceed as follows. First, we will establish the set of *all possible* orbits in the scenario by looking at the system for fixed $\alpha = \alpha^\star$. After that, we will investigate rules for determining the subset of existing orbits for any particular value $\alpha < \alpha^\star$.

2.3. Effect of $f_{\mathcal{L}}$, $f_{\mathcal{C}}$ and $f_{\mathcal{R}}$

To get a first intuitive understanding of the system's behavior, let us state how the functions $f_{\mathcal{L}}$, $f_{\mathcal{C}}$ and $f_{\mathcal{R}}$ determine the form of periodic orbits. It turns out that the dynamics of the discontinuous flat top tent map is governed by the following three mechanisms:

M1 a *channel* in the left partition $I_{\mathcal{L}}$, originating from the unstable fixed point at $x = 0$. Each orbit entering the left partition is trapped in the channel formed by the system function and the principal diagonal for a number of iteration steps until it leaves the left partition.

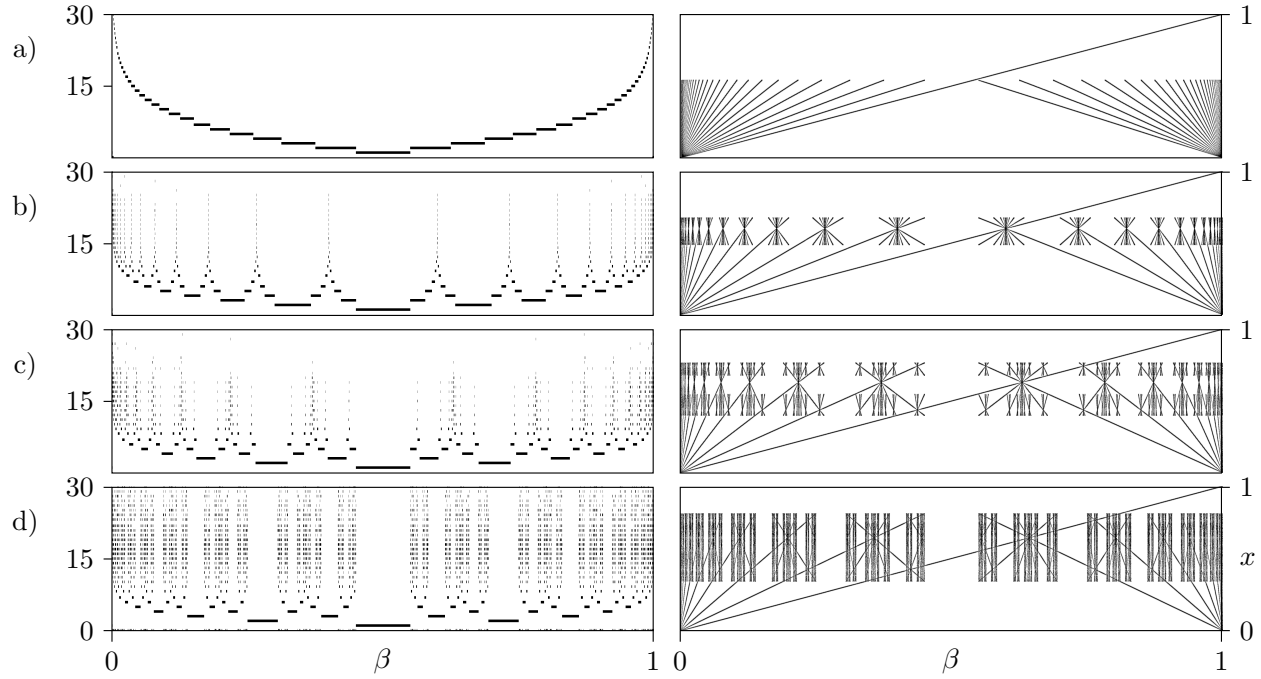

Figure 2: Period diagrams (left) and the corresponding bifurcation diagrams (right) for different values of α (cf. Fig. 3) show the following phenomena: a) pure period incrementing for $\alpha = 0.6$, b) pairs of opposed incrementing cascades in between for $\alpha = 0.75$, c) even further nesting for $\alpha = 0.85$. In d) for $\alpha = 0.9$, a far more complex scenario has evolved.

M2 a *swirl* in the right partition $I_{\mathcal{R}}$, originating from the unstable fixed point[2] $x_{\mathcal{R}}$. Each orbit entering the right partition rotates around this point for a number of iteration steps before leaving the right partition again.

M3 a *'hard reset'* from the center partition $I_{\mathcal{C}}$. As the system function is constant in the center partition, each orbit entering this partition in step n is immediately reset to the value $x_{n+1} = \beta$.

It is worth noticing that M3 implies that each periodic orbit visiting the center partition is super-stable, which offers certain numerical advantages. In particular (see Lemma 1 below), from any initial value located in this partition, for example $x_0 = \frac{1}{2}$, the system is guaranteed to reach the asymptotic dynamics exactly, within one transient iteration step.

3. Dynamics at $\alpha = \alpha^\star$

To get a condensed description of the system's behavior, we can use a symbolic notation based on the letters $\mathcal{L}$, $\mathcal{C}$ and $\mathcal{R}$, corresponding to the three disjoint partitions $I_{\mathcal{L}}$, $I_{\mathcal{C}}$ and $I_{\mathcal{R}}$, as shown in Fig. 1. More precisely, to each n-periodic orbit $(x_0, x_1, \ldots, x_{n-1})$ we define the corresponding symbolic sequence $\sigma = \sigma_0\sigma_1 \ldots \sigma_{n-1}$, such that

$$\sigma_i = \begin{cases} \mathcal{L} & \text{if} \quad x_i \in I_{\mathcal{L}} \\ \mathcal{C} & \text{if} \quad x_i \in I_{\mathcal{C}} \\ \mathcal{R} & \text{if} \quad x_i \in I_{\mathcal{R}}. \end{cases} \tag{9}$$

We can simplify this description for the investigation of stable periodic orbits, as the form of (1) poses the following restrictions.

Lemma 1. *Assume conditions (5) and (6), then an n-periodic orbit* $(x_0, \ldots, x_{n-1})$ *of map (1) is stable if and only if* $\exists\, i \in \{0, \ldots, n-1\}$ *s.t.* $x_i \in I_{\mathcal{C}}$

[2]Note that this fixed point exists only for $\alpha > \alpha_1$. Thus, this mechanism is active only for $\alpha > \alpha_1$.

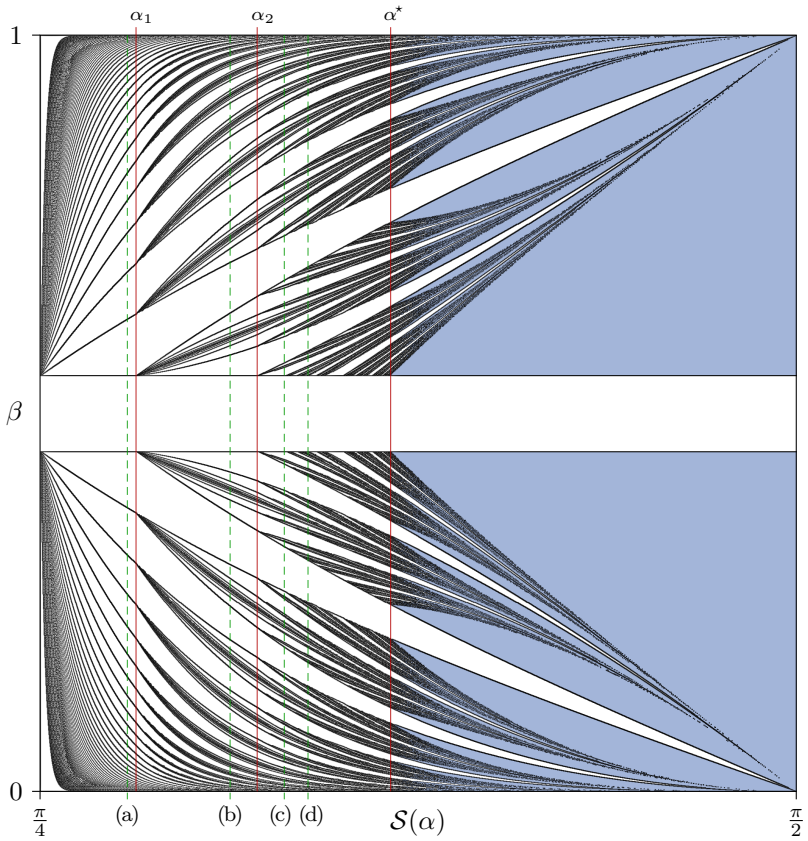

Figure 3: 2D bifurcation structure of (1) in the (α, β)-plane, for $\gamma = 0.1$ and $\alpha \in \left(\frac{1}{2}, \infty\right)$, via the transform $\mathcal{S}(\alpha) = \arctan(2\alpha)$. At α_1 the swirl emerges (see below). At $\alpha^\star$ the escape region emerges. In the blue parameter regions, the typical orbits diverge. The labels (a,b,c,d) indicate the locations of the bifurcation scenarios in Fig. 2.

Proof. Consider the symbolic sequence $\sigma = \sigma_0 \dots \sigma_{n-1}$ corresponding to the orbit $(x_0, \dots, x_{n-1})$ as defined by Eq. (9) and the nth iterated function $f_\sigma = f_{\sigma_0\sigma_1\dots\sigma_{n-1}} = f_{\sigma_{n-1}} \circ \dots \circ f_{\sigma_0}$ with $\sigma_i \in \{\mathcal{L}, \mathcal{C}, \mathcal{R}\}$, $i = 0, \dots, n-1$. Then the derivative of f_σ evaluated at every periodic point x_j, $j = 0, \dots, n-1$ is given by

$$\left.\frac{\mathrm{d}}{\mathrm{d}x} f_\sigma(x)\right|_{x=x_j} = \begin{cases} \pm(2\alpha)^n & \text{if} \quad \sigma_i \in \{\mathcal{L}, \mathcal{R}\}\ \forall\, i = 0, \dots, n-1 \\ 0 & \text{if} \quad \exists\, i \ \text{ s.t. } \ \sigma_i = \mathcal{C} \end{cases} \tag{10}$$

and $\alpha > \frac{1}{2}$ implies $(2\alpha)^n > 1$. As the stability of the orbit $(x_0, \dots, x_{n-1})$ is determined by the stability of the fixed point of f_σ, the orbit is stable if and only if the sequence σ contains a letter $\mathcal{C}$, that means the orbit contains a point in the middle partition. □

Lemma 2. *An n-periodic orbit $(x_0, \dots, x_{n-1})$ of map (1) cannot contain more than one point $x_i \in I_\mathcal{C}$.*

Proof. Assume $x_i, x_j \in I_\mathcal{C}$ where $i \neq j$, then $x_{(i+1) \bmod n} = x_{(j+1) \bmod n} = \beta$. Thus, the considered orbit contains a periodic sub-sequence of period less than n. □

This leads us to the following result:

Theorem 1. *Assume conditions (5) and (6), then each symbolic sequence corresponding to a stable periodic orbit of map (1) contains the symbol $\mathcal{C}$ exactly once.*

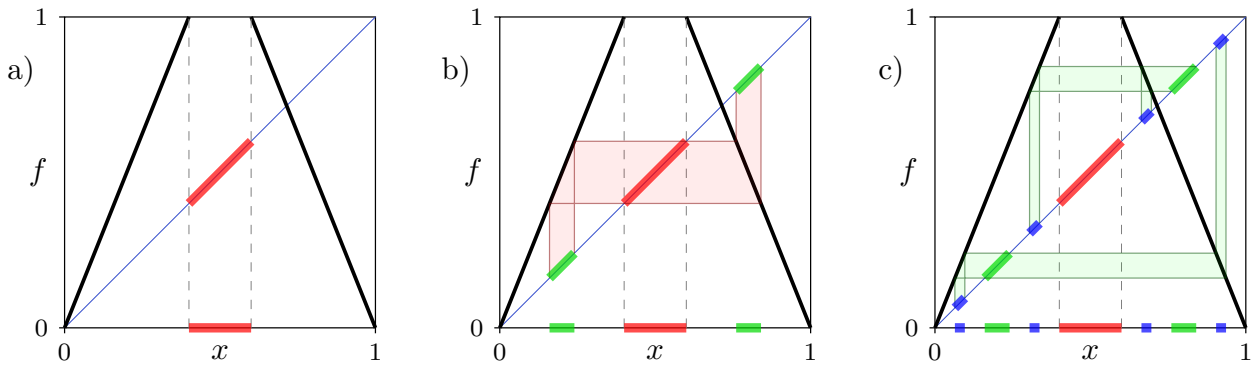

Figure 4: Interval $I_{\mathcal{C}}$ (a) along with its first order (b) and second order (c) preimages at $\alpha^\star$.

Consequently, for every stable periodic orbit we can choose as its symbolic description the sequence where $\mathcal{C}$ is the *first* symbol, and any of the remaining symbols in the sequence is either $\mathcal{L}$ or $\mathcal{R}$. With this definition, $\mathcal{C}$ becomes obsolete as a symbol. Accordingly, we can omit the letter $\mathcal{C}$ in the symbolic description of stable periodic orbits.

Definition 1 ($\mathcal{C}$-reduced sequence)**.** *To each symbolic sequence σ which contains the symbol $\sigma_k = \mathcal{C}$ exactly once (and thus corresponds to one period of a stable orbit of period n), we define the* $\mathcal{C}$-reduced sequence *as*

$$\varrho = \varrho_1 \dots \varrho_{n-1} = \sigma_{k+1} \dots \sigma_{n-1} \sigma_0 \dots \sigma_{k-1}. \tag{11}$$

This essentially leaves us with a simple $\{\mathcal{L}, \mathcal{R}\}$-description for stable periodic orbits, as long as we keep in mind that

- $\mathcal{C}$-reduced sequences are *not* shift-invariant and
- each orbit of period n corresponds to a unique $\mathcal{C}$-reduced sequence with $n-1$ letters.

This means, for example, that there are four distinct $\mathcal{C}$-reduced sequences corresponding to period-3-orbits: $\mathcal{LL}$, $\mathcal{LR}$, $\mathcal{RR}$ and $\mathcal{RL}$. Also, we denote the $\mathcal{C}$-reduced sequence corresponding to a fixed point in the flat interval with the empty word ε. Note also that, as a result of Lemma 1, this convention cannot be used to describe unstable periodic orbits of (1), as it relies on the occurrence of a point $x \in I_{\mathcal{C}}$. However, as our main concern in this work is with the stable periodic orbits, we will treat them in terms of $\mathcal{C}$-reduced sequences in the following, unless stated otherwise.

3.1. The Set of Possible Sequences

Now let us interpret the mechanisms M1–3 introduced in Sec. 2 with respect to the symbolic sequences. The channel (M1) permits an arbitrary number of steps in the left partition, which corresponds to a sub-sequence $\mathcal{LL} \dots \mathcal{L}$. As the fixed point $x_{\mathcal{L}}$ is unstable, the orbit is bound to leave the channel at some point. Recall that $f_{\mathcal{L}}$ is surjective for $\alpha = \alpha^\star$, so the orbit may thereafter land on any point of either the $\mathcal{C}$-partition — in which case the orbit closes — or the $\mathcal{R}$-partition. Here the swirl (M2) comes into action, where the same arguments are applicable as for the channel. Thus, the swirl generates a sub-sequence $\mathcal{RR} \dots \mathcal{R}$, followed by either M1 or M3. Finally, the reset mechanism (M3) closes the orbit and determines its initial value $x_0 = \beta$, and by that also the first symbol of the sequence.

This brief overview suggests that the interplay of swirl and channel could generate arbitrary sequences of the letters $\mathcal{L}$ and $\mathcal{R}$. To be precise, it should be able to produce all 2^{n-1} distinct $\{\mathcal{L}, \mathcal{R}\}$-sequences of length $n-1$ corresponding to stable periodic orbits of period n. In fact we are able to state

Theorem 2. *Assume condition (6) and $\alpha = \alpha^\star$, $n \geq 1$. Then for every $\mathcal{C}$-reduced sequence ϱ of length $n-1$, there exists an interval $I_\varrho \subset [0,1]$ so that for any $\beta \in I_\varrho$ map (1) has a stable n-periodic orbit corresponding to this symbolic sequence.*

For an intuitive explanation of this fact, we consider some stable orbit with the following graphical representation:

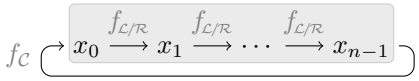

As can be seen, the point x_{n-1} is chosen to lie in the partition $I_{\mathcal{C}}$ in this case. This implies, of course, that the value of x_0 depends solely on the parameter β, whereas the remaining iteration steps depend solely on α. These parameters, however, can be varied independently of each other. When setting β to a *preimage* of x_0 (the former 'initial' value of the orbit) we see that the map now possesses this stable orbit:

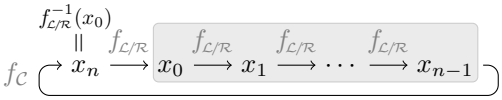

As one can see, we have inserted an extra iteration step by suitably changing β. The point x_{n-1} is still in $I_{\mathcal{C}}$, but the next point was changed to the new x_n. The following iteration, however, brings us back to x_0, as this is precisely how β was chosen. The rest of the orbit remains identical, as this part does not depend on α.

Let us state this thought more formally in the following

Lemma 3. *Assume conditions (5), (6) and*

$$\beta' \in \big[0, \alpha(1-\gamma)\big]. \tag{12}$$

If for $\beta = \beta'$ the map (1) has a stable orbit of period $n \geq 1$ with the $\mathcal{C}$-reduced sequence

$$\varrho' = \varrho_1 \dots \varrho_{n-1} \tag{13}$$

then for $\beta = \beta'' = f_\lambda^{-1}\big(\beta'\big)$, $\lambda \in \{\mathcal{L}, \mathcal{R}\}$ there is a stable orbit of period $n+1$ with the $\mathcal{C}$-reduced sequence

$$\varrho'' = \lambda\varrho'. \tag{14}$$

Proof. For an arbitrary $\alpha > 0$ the inverses of $f_{\mathcal{L}}$ and $f_{\mathcal{R}}$ are given by:

$$f_{\mathcal{L}}^{-1} : \big[0, \alpha(1-\gamma)\big] \to I_{\mathcal{L}}, \qquad x \mapsto \frac{x}{2\alpha} \tag{15}$$

$$f_{\mathcal{R}}^{-1} : \big[0, \alpha(1-\gamma)\big] \to I_{\mathcal{R}}, \qquad x \mapsto 1 - \frac{x}{2\alpha} \tag{16}$$

Consequently, every point $x \in \big[0, \alpha(1-\gamma)\big]$ possesses the two distinct preimages $f_{\mathcal{L}}^{-1}(x)$ and $f_{\mathcal{R}}^{-1}(x)$ under (1). Condition (12) ensures that these two preimages exist for our particular choice of β'.

For the special case $n = 1$ the result is obvious: we know that for $\beta = \beta' \in I_{\mathcal{C}}$ there exists a fixed point corresponding to $\varrho' = \varepsilon$. Therefore, for $\beta = \beta'' = f_{\mathcal{L}}^{-1}(\beta')$ and for $\beta = \beta'' = f_{\mathcal{R}}^{-1}(\beta')$ there are period-2 orbits corresponding to $\mathcal{L}$ and $\mathcal{R}$, respectively. Now let us consider the general case $n \geq 2$ and assume that $\beta = \beta'$ is in the interval $\big[0, \alpha(1-\gamma)\big]$ such that a stable periodic orbit $(x_0 \dots x_{n-1})$ with the $\mathcal{C}$-reduced sequence ϱ' exists, which means

$$x_0 = f_{\mathcal{C}}\big(f_{\varrho'}(x_0)\big), \quad x_0 = \beta'. \tag{17}$$

Now we consider $\beta'' = f_{\mathcal{L}}^{-1}(\beta')$, i.e. one of the two preimages of β'. By setting β to β'' in (1) and $x_0 = \beta'$, we see that the points $x_0, \dots, x_{n-1}$ remain as above, but

$$x_n = f_{\mathcal{C}}(x_{n-1}) = \beta''. \tag{18}$$

Using the fact that $\beta'' \in I_{\mathcal{L}}$ and $f_{\mathcal{L}}\big(\beta''\big) = \beta'$ we get

$$x_0 = f_{\mathcal{L}}\Big(f_{\mathcal{C}}\big(f_{\varrho'}(x_0)\big)\Big). \tag{19}$$

The symbolic sequence corresponding to this stable periodic orbit thus reads $\sigma'' = \varrho'\mathcal{C}\mathcal{L}$. By application of Definition 1 we get the new $\mathcal{C}$-reduced sequence $\varrho'' = \mathcal{L}\varrho'$. This shows that for $\beta = \beta''$ the system has a stable orbit of period $n+1$ with the $\mathcal{C}$-reduced sequence $\mathcal{L}\varrho'$. Likewise, if we set $\beta'' = f_{\mathcal{R}}^{-1}(\beta')$, we get an orbit with $\varrho'' = \mathcal{R}\varrho'$. □

With $\alpha = \alpha^\star$ as defined in (4), condition (12) simplifies to $\beta' \in [0,1]$. Thereby, every point in the unit interval has two preimages under (1), which is also indicated in Fig. 4. It follows that, for $\alpha = \alpha^\star$, Lemma 3 is applicable for every stable orbit existing in the investigated parameter domain. This is the basic requirement for the following inductive proof of Theorem 2, which we stated above.

Proof of Theorem 2.
Basis: We know that a fixed point $x = \beta$ exists for every $\beta \in I_{\mathcal{C}}$. The corresponding sequence is $\varrho_1^1 = \varepsilon$.
Inductive step: For $\alpha = \alpha^\star$, Lemma 3 is applicable for any $\beta' \in [0,1]$, which implies the following: If a periodic orbit with sequence ϱ exists for some $\beta' \in [0,1]$, then so do two distinct orbits with the sequences $\mathcal{L}\varrho$ (which exists for $\beta = f_{\mathcal{L}}^{-1}(\beta') \in I_{\mathcal{L}}$) and $\mathcal{R}\varrho$ (which exists for $\beta = f_{\mathcal{R}}^{-1}(\beta') \in I_{\mathcal{R}}$). All possible sequences (and the corresponding domains[3]) follow by recursive application of this argument to the sequence $\varrho_1^1 = \varepsilon$. □

So far we proved that at $\alpha = \alpha^\star$ the n-periodic orbits corresponding to all possible 2^{n-1} $\mathcal{C}$-reduced symbolic sequences exist. Additionally, we can make a first statement about their locations in parameter space. For this reason let us number all sequences of the same period according to the order of the corresponding orbits along the β-axis. Let us denote the sequence corresponding to the i-th orbit of period n as ϱ_i^n. So for $n = 1$ there is only one sequence $\varrho_1^1 = \varepsilon$, for $n = 2$ there are two sequences $\varrho_1^2 = \mathcal{L}$ and $\varrho_2^2 = \mathcal{R}$, and so forth. In general, of all 2^{n-1} sequences corresponding to period-n orbits, the sequence whose corresponding orbit appears at the smallest value of β is referred to as ϱ_1^n, and the one with appearing at the largest value is $\varrho_{2^{n-1}}^n$. Note also that the location of the preimages satisfies

$$\left|\frac{1}{2} - f_{\mathcal{L}}^{-1}(x)\right| = \left|\frac{1}{2} - f_{\mathcal{R}}^{-1}(x)\right| = \frac{1}{2}\left(1 - \frac{x}{\alpha^\star}\right), \tag{20}$$

i.e. distance of the preimages to the middle point $x = \frac{1}{2}$ decreases linearly in x. This means that the smallest x has the "outermost", and the largest x the "innermost" preimages. Lemma 3 states that the parameter change $\beta \mapsto f_\lambda^{-1}(\beta)$, $\lambda \in \{\mathcal{L}, \mathcal{R}\}$ is equivalent to the sequence change $\varrho \mapsto \lambda\varrho$. The location on the β-axis of the two period-$(n+1)$ orbits corresponding to these two sequences $\mathcal{L}\varrho$ and $\mathcal{R}\varrho$ can be explained easily based on Eq. (20). For example, as the sequence ϱ_1^n has the smallest β-value among all sequences corresponding to period-n orbits, so the sequence $\mathcal{L}\varrho_1^n$ has the smallest β-value among all 2^n sequences corresponding to period-$(n+1)$ orbits, that means $\mathcal{L}\varrho_1^n = \varrho_1^{n+1}$. Similarly, the sequence $\mathcal{R}\varrho_1^n$ has the largest β-value among all sequences corresponding to period-$(n+1)$ orbits, that means $\mathcal{R}\varrho_1^n = \varrho_{2^n}^{n+1}$. In general, all 2^n sequences corresponding to period-$(n+1)$ orbits can be generated from the 2^{n-1} sequences corresponding to period-n orbits recursively according to the following rules.

$$\forall i = 1, \ldots, 2^{n-1}\colon \quad \varrho_i^n \begin{cases} \nearrow & \mathcal{L}\varrho_i^n = \varrho_i^{n+1} \\ \searrow & \mathcal{R}\varrho_i^n = \varrho_{2^n+1-i}^{n+1} \end{cases} \tag{21}$$

Again, the indexes $i = 1, \ldots, 2^n$ of the sequences ϱ_i^{n+1} define the order of the corresponding orbits along the β-axis. In the following this order will be denoted as the *β-ordering* of the sequences.

Note that the rules given by Eq. (21) generate the β-ordering of the sequences corresponding to orbits *with a certain period*, but without making any statement about their relative ordering to the sequences of any other period. However, what we need in order to explain the bifurcation structure occurring at $\alpha = \alpha^\star$ is the β-ordering of *all* sequences, regardless of their period. In particular, it is not sufficient to state that

[3]Due to the strict monotonicity of $f_{\mathcal{L}}^{-1}$ and $f_{\mathcal{R}}^{-1}$, these domains remain intervals in each step.

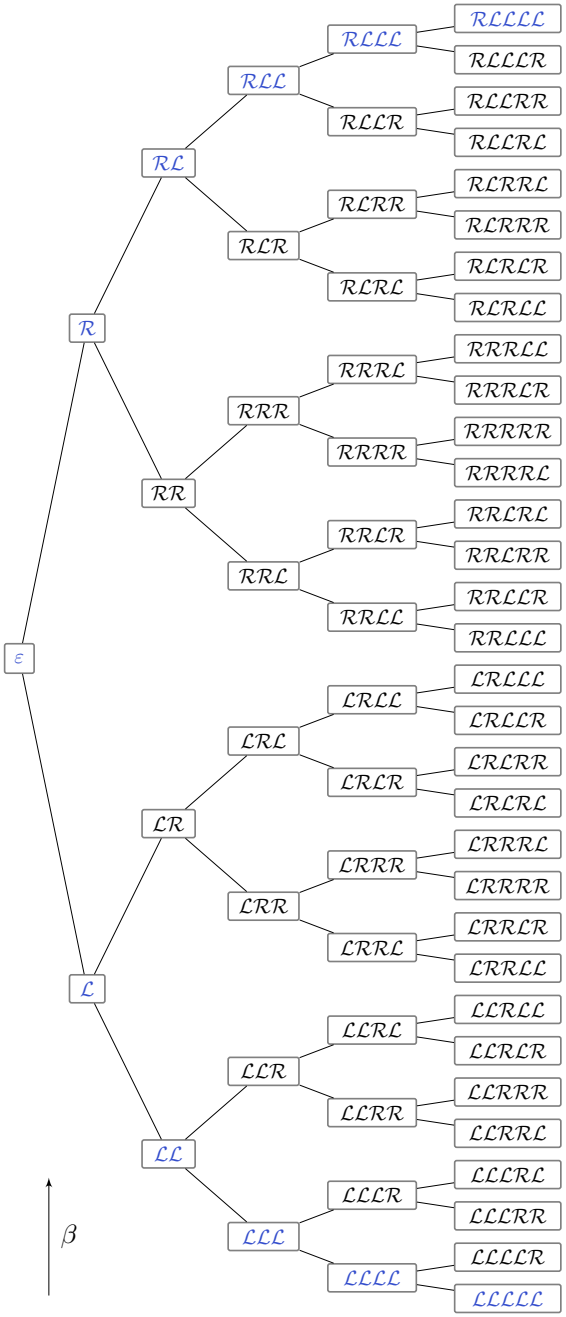

Figure 5: The full binary tree of periodic symbolic sequences up to period 6. The β-ordering is indicated by the arrow. The outermost sequences compose the 'minimal' tree for $\alpha < \alpha_1$ (cf. Figs. 2a and 3).

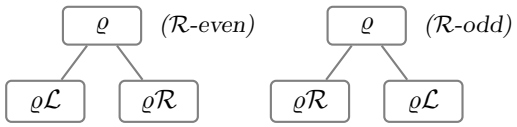

Figure 6: The Suffix Rules generate period $n+1$ sequences from period n sequences: if ϱ contains an even number of $\mathcal{R}$s, an $\mathcal{L}$ is appended to the left and an $\mathcal{R}$ to the right; otherwise the order is reversed. The resulting orbits are β-ordered from left to right.

the period-n orbit corresponding to the sequence ϱ_i^n can be found between the orbits corresponding to ϱ_{i-1}^n and ϱ_{i+1}^n, since we also need to know how these orbits are located with respect to the period-$(n-1)$ orbits.

The β-ordering of all sequences can be determined by arranging all sequences in a binary tree structure, where each level of the tree contains the sequences of the corresponding period. The relationship in this tree is such that the children of a particular node are the sequences of the next higher period, which are located the nearest along β in parameter space. The tree of symbolic sequences up to period $n = 6$ is shown in Fig. 5. This tree is generated by recursive application of the following rules:

S1 Start by defining the root node with the sequence $\varrho = \varepsilon$.

S2 To each node where ϱ contains an *even* number of $\mathcal{R}$s, add left child with sequence $\varrho\mathcal{L}$, and right child with sequence $\varrho\mathcal{R}$.

S3 To each node where ϱ contains an *odd* number of $\mathcal{R}$s, add left child with sequence $\varrho\mathcal{R}$, and right child with sequence $\varrho\mathcal{L}$.

We denote these rules as the *Suffix Rules*, which are also illustrated in Fig. 6 for clarity. Note that the Suffix Rules add a letter at the end of a sequence, whereas the rules given by Eq. (21) add a letter in front. It is also worth to emphasize that the Suffix Rules differ from Eq. (21), since in the binary tree the sequences corresponding to orbits *up to a certain period* are generated according to their β-ordering. It is clear that by recursive appending of both $\mathcal{L}$ and $\mathcal{R}$, all anticipated sequences will be produced. Note that these rules were already mentioned in [15], in the context of the logistic map, where the location of symbolic sequences along the interval of initial values is investigated. Although not surprisingly, this fact points out that the discontinuous flat top tent map, being not unimodal in the strong sense, has still some similarities with the usual unimodal maps.

It is worth mentioning here, that for the case $\alpha = \alpha^\star$ we can use the argument provided in the proof of Theorem 2 to compute the interval for the parameter β where a stable periodic orbit corresponding to any given sequence ϱ exists. As we know, the stable fixed point with $\varrho = \varepsilon$ exists for $\beta \in U_\varepsilon = I_\mathcal{C}$. Consequently, the existence region of the orbit with $\varrho = \varrho_1\varrho_2\ldots\varrho_{n-1}$ is determined by the order-$(n-1)$ preimage

$$U_\varrho = f_\varrho^{-1}(I_\mathcal{C}) = f_{\varrho_1}^{-1} \circ f_{\varrho_2}^{-1} \circ \ldots \circ f_{\varrho_{n-1}}^{-1}(I_\mathcal{C}) \tag{22}$$

of that of the fixed point. This means, given that $\alpha = \alpha^\star$, the n-periodic orbit with the sequence ϱ exists if and only if $\beta \in U_\varrho$ as determined by (22).

For the sake of completeness, we may ask which part of the parameter space is covered by the existence regions of the orbits described so far. An answer to this question is given by the following theorem:

Theorem 3. *Assume condition (6) and $\alpha = \alpha^\star$, then map (1) possesses a stable periodic orbit with a sequence generated by the Suffix Rules for any parameter value $\beta \in [0,1]$, except on a set of Lebesgue measure zero.*

Proof. The parameter region $\beta \in I_\mathcal{C}$ (where a stable fixed point exists) covers a fraction γ of the interval $[0,1]$ by definition, and leaves a fraction $1-\gamma$ uncovered. As for $\alpha = \alpha^\star$

$$\begin{aligned} f_\mathcal{L} : I_\mathcal{L} &\to [0,1], \text{ invertible,} \\ f_\mathcal{R} : I_\mathcal{R} &\to [0,1], \text{ invertible,} \\ I_\mathcal{L} \cap I_\mathcal{R} = \emptyset, &\text{ and } [0,1] \setminus I_\mathcal{C} = I_\mathcal{L} \cup I_\mathcal{R}, \end{aligned} \tag{23}$$

there exist two preimages of $I_{\mathcal{C}}$, each of which again covers a fraction γ of $I_{\mathcal{L}}$ and $I_{\mathcal{R}}$, due to the linearity of $f_{\mathcal{L}}$ and $f_{\mathcal{R}}$. In other words, the first order preimages of $I_{\mathcal{C}}$ cover a fraction γ of the fraction $1-\gamma$ which was not covered in the previous step by the middle partition $I_{\mathcal{C}}$. In total, this represents a fraction $\gamma(1-\gamma)$ of the interval $[0,1]$. These preimages are, of course, the existence regions of the period-2 orbits with the sequences $\mathcal{L}$ and $\mathcal{R}$. This argument is applicable recursively for higher order preimages. Thus, the nth order preimages of $I_{\mathcal{C}}$ cover a fraction $\gamma\big(1-\gamma\big)^n$ of the unit interval. So for the fraction of $[0,1]$ covered by the union

$$S = \bigcup_{n=0}^{\infty} f^{-n}\big(I_{\mathcal{C}}\big) \tag{24}$$

of $I_{\mathcal{C}}$ and all of its preimages, we get in the limit

$$\sum_{n=0}^{\infty} \gamma\big(1-\gamma\big)^n = \gamma \cdot \frac{1}{1-\big(1-\gamma\big)} = 1, \tag{25}$$

i.e. the closure of S is $\overline{S} = [0,1]$. □

This argument is also indicated graphically in Fig. 4. Although we constructed the set S in parameter space ($\beta \in S$), we can also regard this set in *state space* as the set of all points that eventually get mapped to $I_{\mathcal{C}}$. In order to avoid confusion, we shall in the following refer to the set S in parameter space, such that $\beta \in S$, whereas the notation $\widetilde{S}$ is used for the same set in state space, and accordingly $x \in \widetilde{S}$.

This leads us directly to the following assertions, given that we choose the parameter values within the region established in Sec. 2.1.

Corollary 1. *Assume condition (6) and $\alpha = \alpha^\star$, then the stable set W^s of the periodic orbit intersecting $I_{\mathcal{C}}$ is $\widetilde{S}$.*

Recall that for a fixed point x^* of a map f the stable set is defined by $W^s(x^*) := \{x \mid \lim_{i\to+\infty} f^i(x) = x^*\}$. Accordingly, the stable set of a n-periodic orbit is given by the union of the stable sets of all points of the orbit considered as n fixed points of the iterated map f^n. As shown in (25), $\widetilde{S}$ is dense in $[0,1]$. Therefore, we can also state

Corollary 2. *Assume condition (6) and $\alpha = \alpha^\star$, then the orbit intersecting $I_{\mathcal{C}}$ is the unique attractor of (1).*

Note also that the construction of S implies that its complement $M = [0,1] \setminus S$ is a Cantor set (For example, for $\gamma = \frac{1}{3}$, M is the famous *middle-third* Cantor set). Equivalently to the sets S and $\widetilde{S}$, we shall distinguish in the following between sets M in parameter space and $\widetilde{M} = [0,1] \setminus \widetilde{S}$ in state space. In parameter space, the set M consists of the accumulation points of the nested period incrementing scenario. As for β tending from both sides to a point $\beta \in M$ the periods tend to infinity, one could assume that for $\beta \in M$ the dynamics must be quasiperiodic (similar to the case of the period adding scenario associated with the well-known Farey-like structures). However, this assumption is incorrect, as we will demonstrate in the next section.

3.2. Milnor Attractors

So far we considered only stable periodic orbits. We already know of two particular *unstable* periodic orbits, namely the fixed points at $x_{\mathcal{L}} = 0$ and at $x_{\mathcal{R}} = \frac{2\alpha}{2\alpha+1}$. It is easy to show that, for $\alpha = \alpha^\star$, the discontinuous flat top tent map actually possesses a countable infinity of unstable periodic orbits, as well as an uncountable infinity of aperiodic orbits, which can be uniquely identified by corresponding (respectively terminating and non-terminating) symbolic sequences.

Theorem 4. *Assume condition (6) and $\alpha = \alpha^\star$, $n \geq 1$. Then for every (not $\mathcal{C}$-reduced) sequence $\sigma = \sigma_0\sigma_1\ldots\sigma_{n-1}$ with $\sigma_i \in \{\mathcal{L},\mathcal{R}\}$, map (1) has a unique unstable orbit with this symbolic sequence.*

Proof. Consider the nth iterated function $f_\sigma = f_{\sigma_0\sigma_1\ldots\sigma_{n-1}} = f_{\sigma_{n-1}} \circ \ldots \circ f_{\sigma_0}$ with $\sigma_i \in \{\mathcal{L}, \mathcal{R}\}$. As for $\alpha = \alpha^\star$ the functions

$$f_\mathcal{L} : I_\mathcal{L} \to [0,1], \qquad f_\mathcal{R} : I_\mathcal{R} \to [0,1], \tag{26}$$

are both linear, and of course $I_\mathcal{L}, I_\mathcal{R} \subset [0,1]$, it follows immediately that the function

$$f_\sigma : U_\sigma \to [0,1], \tag{27}$$

is also linear, with $U_\sigma = f_\sigma^{-1}\big([0,1]\big) \subset [0,1]$. Thus, each of these iterates has exactly one fixed point $x \in U_\sigma$ with $x = f_\sigma(x)$, which corresponds to an unstable orbit of (1) with the sequence σ (cf. Lemma 1). □

Note that the sequences corresponding to unstable orbits are not $\mathcal{C}$-reduced and therefore shift-invariant.

Corollary 3. *Assume condition (6) and $\alpha = \alpha^\star$, then map (1) possesses a countable infinity of unstable periodic orbits.*

Proof. If we take n to be arbitrarily large but *finite*, the set of orbits resulting from Theorem 4 is of equal cardinality as the set of all terminating $\{\mathcal{L}, \mathcal{R}\}$-sequences, and therefore countably infinite. □

Corollary 4. *Assume condition (6) and $\alpha = \alpha^\star$, then map (1) possesses an uncountable infinity of aperiodic orbits.*

Proof. In the limit $n \to \infty$, the set of orbits resulting from Theorem 4 is of equal cardinality as the set of all *non*-terminating $\{\mathcal{L}, \mathcal{R}\}$-sequences, and therefore *un*countably infinite, due to Cantor's Second Diagonal Argument. □

From Theorem 3 we now know which orbits exist for any $\beta \in S$. Now we can also state what happens if β lies within the zero measure set M. For this, we regard the behavior of the tent map

$$x_{n+1} = \begin{cases} 2\alpha x_n & \text{if} \quad x_n \leq \frac{1}{2} \\ 2\alpha(1 - x_n) & \text{if} \quad x_n > \frac{1}{2} \end{cases} \tag{28}$$

for $\alpha = \alpha^\star$. Eq. (4) implies that $\alpha^\star > 1$, so whereas (1) and (28) are identical on the partitions $I_\mathcal{L}$ and $I_\mathcal{R}$, the tent map possesses an escape interval at $I_\mathcal{C}$. That means that all orbits started at $x_0 \in \widetilde{S}$, i.e. on the escape interval or one of its preimages, diverge under the dynamics of the tent map. For all other orbits with $x_0 \in \widetilde{M}$, the behavior of the tent map and the discontinuous flat top tent map is identical. It is known that the non-diverging orbits of the tent map for $\alpha > 1$ are exactly those, which are mentioned in Theorem 4 and corollaries.

It is worth noting that the behavior in the generic case $\beta \in S$ is quite different from the behavior in the special case $\beta \in M$. In the former case, an orbit started at a typical initial value $x_0 \in \widetilde{S}$ converges to the unique stable periodic orbit. All unstable periodic orbits located in the set $\widetilde{M}$ coexist with this unique stable periodic orbit. Also, the stable set W^s of each unstable orbit is a subset of $\widetilde{M}$. So in this case the stable set of each unstable orbit is of zero measure.

For $\beta \in M$ on the other hand, the situation is different. In this case, an orbit started at a typical initial value $x_0 \in \widetilde{S}$ will be mapped to some point $x \in \widetilde{M}$ and eventually to one of the unstable (periodic or aperiodic) orbits. Therefore, the stable set W^s of *this particular* unstable orbit includes $\widetilde{S}$ and is therefore dense in $[0,1]$. In this case the unstable orbit is the only attracting invariant set[4] of map (1). Attracting invariant sets of this kind, commonly referred to as Milnor attractors, are examined e.g. in [16] and represent locally unstable invariant sets whose stable sets have a positive Lebesgue measure. Therefore, we can state the following

[4]To be precise, the aperiodic orbits can not be regarded as attractors, since they represent open sets and an attractor is per definition a closed set. In this case, the attractor is given by the closure of the aperiodic orbit.

Theorem 5. *Assume condition (6) and $\alpha = \alpha^\star$, then for $\beta \in M$ the unique attractor of map (1) is a (periodic or aperiodic) Milnor attractor.*

So far we demonstrated that at $\alpha = \alpha^\star$ stable periodic, unstable periodic and aperiodic orbits exist corresponding to all possible symbolic sequences, and investigated their location in parameter space with respect to each other. For $\alpha > \alpha^\star$ the situation is qualitatively equal to that described in the previous section, with the addition of diverging orbits. Indeed, Theorems 2 and 4 are valid for any $\alpha > \alpha^\star$, therefore no new orbits can emerge and none of the present orbits can vanish for increasing α. By contrast, Theorem 3 is no longer valid for $\alpha > \alpha^\star$, as in this case there are initial values x_0 for which the orbits leave the interval $[0, 1]$ and diverge. It can be seen that for increasing α the fraction of the interval $[0, 1]$ covered by these initial values increases, so that for $\alpha \to +\infty$ the complete bifurcation structure shrinks to two organizing centers in the (α, β) plane (codimension-two big bang bifurcation points), namely $(+\infty, 0)$ and $(+\infty, 1)$, as shown in Fig. 3.

4. Dynamics for $\alpha < \alpha^\star$

4.1. Subsets of Existing Sequences

So far the behavior of discontinuous flat top tent map for $\alpha \geq \alpha^\star$ is explained. In the next step we have to investigate the case $\alpha < \alpha^\star$. In this case much less periodic orbits exist, as can already be seen in Figs. 2a and b, and hence not every sequence is possible. To understand the reason for this, recall Eq. (22), which we used in Sec. 3.1 to calculate the existence region of any sequence in the case $\alpha = \alpha^\star$. A necessary condition for the validity of this equation is the invertibility of $f_\mathcal{L}$ and $f_\mathcal{R}$, a fact that was given for $\alpha = \alpha^\star$. More precisely, it must be guaranteed that each preimage along the "inversion chain" in Eq. (22) lies within the proper domain, i.e.

$$f^{-1}_{\varrho_{n-1}}\big(I_\mathcal{C}\big) \subseteq I_{\varrho_{n-1}}, \quad \text{and} \quad f^{-1}_{\varrho_{n-2}} \circ f^{-1}_{\varrho_{n-1}}\big(I_\mathcal{C}\big) \subseteq I_{\varrho_{n-2}}, \tag{29}$$

and so on. As for $\alpha < \alpha^\star$ the preimage of $[0, 1]$ under $f_{\mathcal{L}/\mathcal{R}}$ may be considerably larger than $I_{\mathcal{L}/\mathcal{R}}$, this is no longer given. In order to be able to compute the existence regions of sequences for $\alpha < \alpha^\star$, we must require that the inverses are restricted to the corresponding domains $I_{\mathcal{L}/\mathcal{C}/\mathcal{R}}$:

$$f^{-1}_\lambda(\cdot) := f^{-1}_\lambda(\cdot) \cap I_\lambda, \tag{30}$$

in which case (22) may well produce $U_\varrho = \emptyset$ for certain ϱ and α, with $\lambda = \varrho_i$ for some $i \in 1 \ldots n-1$. Consequently, this would imply that, for the particular choice of α, the orbit corresponding to the sequence ϱ does not exist.

Now, for a given value $\alpha < \alpha^\star$, we can determine the symbolic sequences of all existing stable periodic orbits in the following way. First we calculate the full binary tree of symbolic sequences according to the Suffix Rules. Then we remove those nodes, for which $U_\varrho = \emptyset$. What remains is a collection of nodes with the sequences that actually exist for the chosen α in the correct β-order. However, this approach has a significant disadvantage, because the resulting graph may become disconnected, as can be clearly seen in Fig. 8a. To understand why this is the case, we return to the 2D bifurcation structure and consider the situation shown in Fig. 7, where the existence regions of the three particular sequences $\mathcal{RRL}$, $\mathcal{RRLL}$ and $\mathcal{RRLR}$ are highlighted. According to the Suffix Rules, the nodes in the binary tree corresponding to the latter two sequences are the children of the node corresponding to the former one. Note that of these three sequences, the bifurcation scenario at $\alpha = 0.9$ (indicated by the dashed line) intersects only the existence region of the sequence $\mathcal{RRLR}$, whereas the existence region of its parent sequence $\mathcal{RRL}$ is *not* intersected. As a consequence, when we generate the set of all sequences existing at the parameter value $\alpha = 0.9$ by the procedure introduced above, we get several "orphaned" nodes, that means nodes without a parent node, as shown in Fig. 8a. This graph doesn't offer much insight into the systematics determining just which sequences exist and which do not.

As a consequence, when using the Suffix Rules to generate all sequences up to a certain period for a given value of $\alpha < \alpha^\star$, we are forced to generate the *complete* tree of all possible sequences up to this period, and

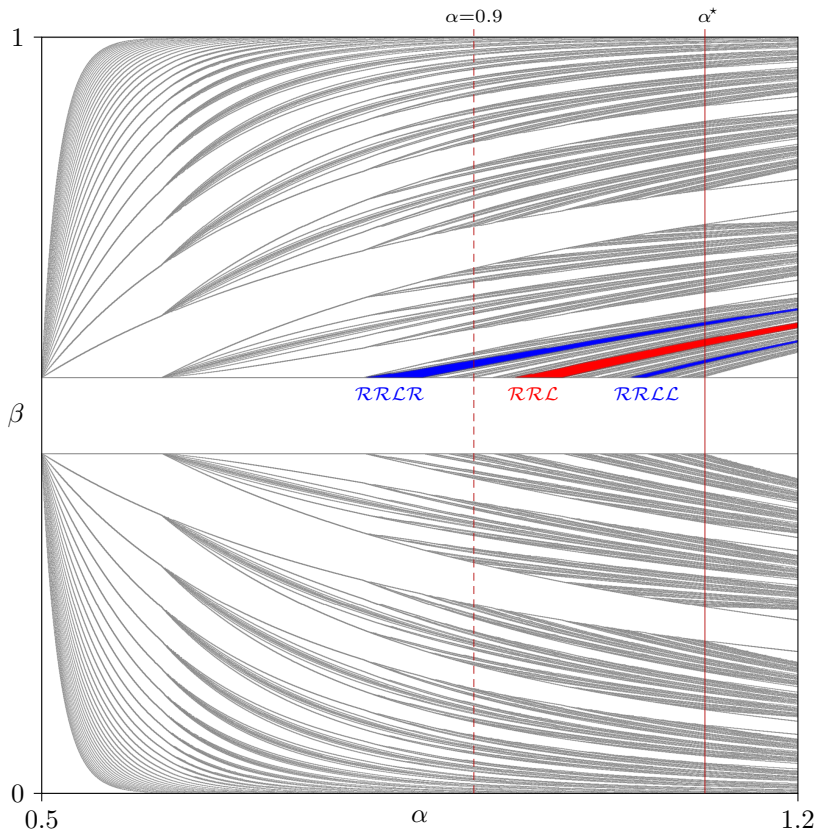

Figure 7: An example showing why, in the binary tree generated by the Suffix Rules, some nodes may become "orphaned". The regions with the sequences $\mathcal{RRL}$, $\mathcal{RRLR}$ and $\mathcal{RRLL}$ are highlighted. Both latter sequences are children of the former under the Suffix Rules, but of these three, only one child exists in the bifurcation scenario at $\alpha = 0.9$ (dashed line).

then *remove* the nodes corresponding to those sequences ϱ with an empty existence region U_ϱ. Therefore, it would be preferable to arrange the set of all existing sequence in a different way, ensuring that the resulting tree is connected. In that case we can interrupt the calculations at every node which corresponds to a sequence with an empty domain.

An example of this alternative approach is shown in Fig. 8b, where the same sequences as in Fig. 8a are organized in a connected tree. In the following section, a set of rules is presented which allows us to generate a connected tree of all sequences which exist for a given value of $\alpha < \alpha^\star$.

4.2. Interval Mapping

As can be seen in the 2D bifurcation structure (cf. Fig. 3), less and less orbits exist for decreasing α. In order to calculate the existence region of the orbit corresponding to a particular sequence, and thereby also to determine whether this orbit exists for a certain value of α, we need to follow up the preimages of the interval $I_\mathcal{C}$ up to the point where there are no further preimages. Following this rather simple idea, a constructive approach for the calculation of the set of all existing sequences for a given value of $\alpha < \alpha^\star$ is presented in this section. This approach makes use of the *interval mapping* technique and allows us to obtain the connected tree, as mentioned in the previous section.

In order to follow the preimages of the complete interval $I_\mathcal{C}$ taking into account the partition constraints of the map let us extend the definition of $f(x)$ by means of interval arithmetic as follows. Let $\mathbb{I}$ be the set of connected subsets of $[0, 1]$. Note that $\mathbb{I}$ also incorporates real numbers $r \in [0, 1]$ in the form of singletons $[r, r] \in \mathbb{I}$. Adopting the nomenclature used in [17], we then denote an arbitrary sub-interval of

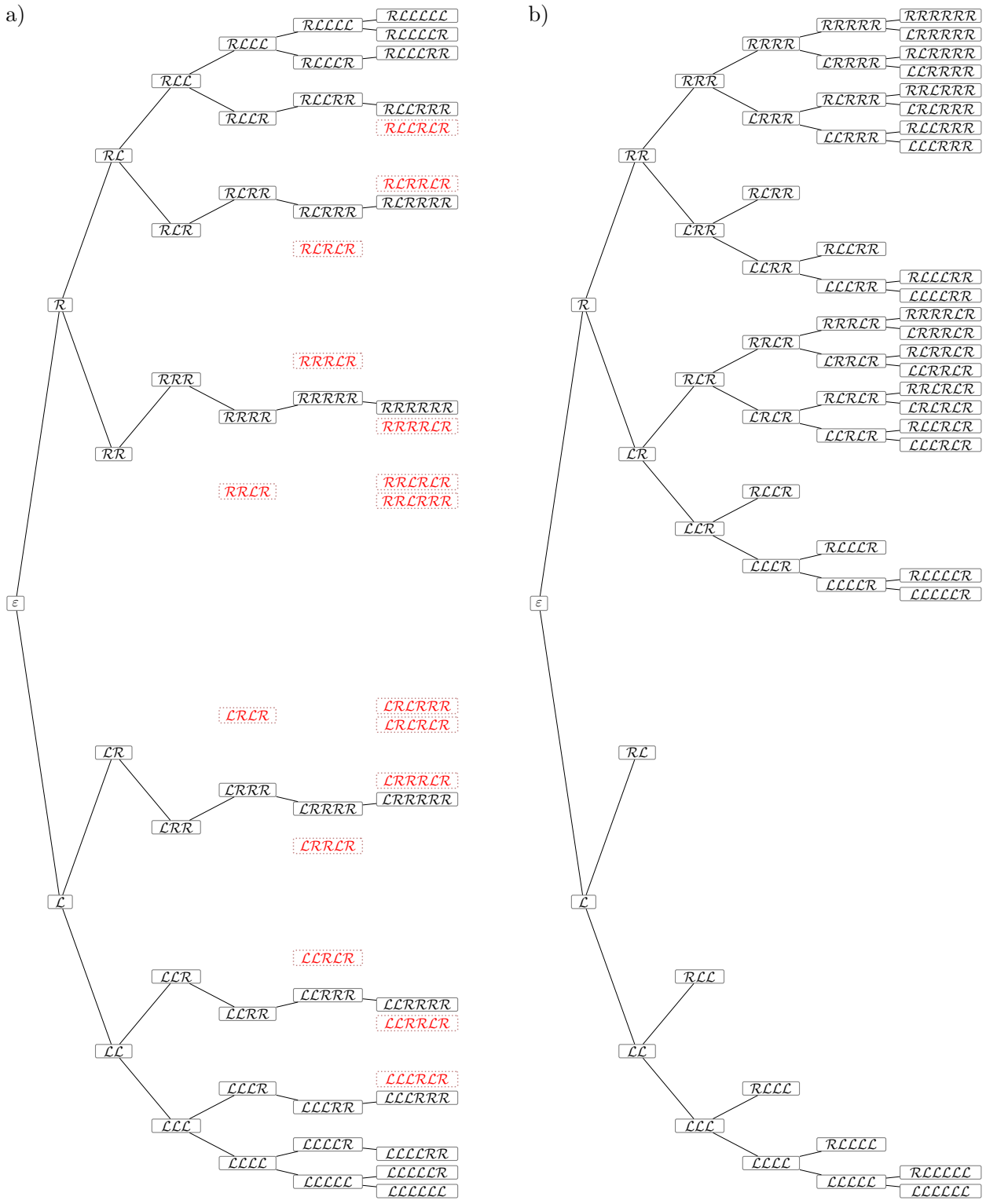

Figure 8: The symbolic sequences corresponding to periodic orbits up to period 7 existing at $\alpha = 0.9$. a) Arrangement according to the Suffix Rules leads to a disconnected tree with orphaned nodes. b) Arrangement of the same sequences according to preimage relationship (i.e. Prefix Rules) gives a connected, albeit unbalanced, tree.

$[0,1]$ as $[x] \in \mathbb{I}$. Recall that such intervals can be operated on using basic interval arithmetic (for instance, $a - [b,c] = [a-c, a-b]$). Thus, instead of the real-valued functions composing the original map

$$f_{\mathcal{L}}, f_{\mathcal{C}}, f_{\mathcal{R}} : I_{\mathcal{L}/\mathcal{C}/\mathcal{R}} \to \mathbb{R} \tag{31}$$

we now consider interval-valued functions

$$\big[f_{\mathcal{L}}\big],\ \big[f_{\mathcal{C}}\big],\ \big[f_{\mathcal{R}}\big] : \mathbb{I} \to \mathbb{I}, \tag{32}$$

which we define as

$$\big[f_{\mathcal{L}}\big]: \qquad [x] \ \mapsto\ \big(2\alpha[x]\big) \cap I_{\text{img}} \tag{33}$$

$$\big[f_{\mathcal{C}}\big]: \quad [x] \ \mapsto \begin{cases} [\beta] & \text{if} \quad [x] \cap I_{\mathcal{C}} \neq \emptyset \\ \emptyset & \text{if} \quad [x] \cap I_{\mathcal{C}} = \emptyset \end{cases} \tag{34}$$

$$\big[f_{\mathcal{R}}\big]: \qquad [x] \ \mapsto\ \Big(2\alpha\big(1 - [x]\big)\Big) \cap I_{\text{img}} \tag{35}$$

where $I_{\text{img}} = \big[0, \alpha(1-\gamma)\big] \cap [0,1]$ is the image of the original functions $f_{\mathcal{L}}$ and $f_{\mathcal{R}}$, clipped to the unit interval. An important effect of this definition is that, for $\lambda \in \{\mathcal{L}, \mathcal{C}, \mathcal{R}\}$,

$$[x] \cap I_{\lambda} = \emptyset \ \Leftrightarrow\ \big[f_{\lambda}\big]\big([x]\big) = \emptyset, \tag{36}$$

which ensures that domain constraints are handled properly. Compare for example $f_{\mathcal{L}}$ and $\big[f_{\mathcal{L}}\big]$. If we naïvely calculate $f_{\mathcal{L}}(x)$ for some value $x \notin I_{\mathcal{L}}$ outside of the functions domain within (1), we get a value which is not relevant for the function f, i.e. $f_{\mathcal{L}}(x) \neq f(x)$ in general. By contrast, if we calculate $\big[f_{\mathcal{L}}\big]\big([x]\big)$ for some interval $\big[x\big]$ with $\big[x\big] \cap I_{\mathcal{L}} = \emptyset$, that means "outside of the functions domain", we get the empty set $\emptyset$ as a result. Any further application of $\big[f\big]$ will also yield the empty set. Thus, domain constraints are taken into account and the calculation remains correct. Due to convexity of I_{img} and monotonicity of $f_{\mathcal{L}/\mathcal{R}}$, $[x]$ remains an interval (although possibly an empty one) under application of (33) and (35). Eq. (34) also yields an element of $\mathbb{I}$, namely the singleton $[\beta]$ or the empty set. It is now an easy task to define pseudo-inverses $\big[f_{\mathcal{L}}^{-1}\big],\ \big[f_{\mathcal{C}}^{-1}\big],\ \big[f_{\mathcal{R}}^{-1}\big] : \mathbb{I} \to \mathbb{I}$ as follows

$$\big[f_{\mathcal{L}}^{-1}\big]: \qquad [y] \ \mapsto\ \big(\tfrac{1}{2\alpha}[y]\big) \cap I_{\mathcal{L}} \tag{37}$$

$$\big[f_{\mathcal{C}}^{-1}\big]: \quad [y] \ \mapsto \begin{cases} I_{\mathcal{C}} & \text{if} \quad [y] \cap [\beta] \neq \emptyset \\ \emptyset & \text{if} \quad [y] \cap [\beta] = \emptyset \end{cases} \tag{38}$$

$$\big[f_{\mathcal{R}}^{-1}\big]: \qquad [y] \ \mapsto\ \big(1 - \tfrac{1}{2\alpha}[y]\big) \cap I_{\mathcal{R}}. \tag{39}$$

Note that

$$[y] \cap I_{\text{img}} \ = \emptyset \quad \Leftrightarrow\ \big[f_{\mathcal{L}/\mathcal{R}}^{-1}\big]\big([y]\big) = \emptyset, \tag{40}$$

$$[y] \cap [\beta] \ = \emptyset \quad \Leftrightarrow\ \big[f_{\mathcal{C}}^{-1}\big]\big([y]\big) = \emptyset. \tag{41}$$

Together with (36) this implies that actual inversion only takes place if $[x] \subseteq I_{\mathcal{L}/\mathcal{R}}$ and $[y] \subseteq I_{\text{img}}$ respectively, or $[x] = I_{\mathcal{C}}$ and $[y] = [\beta]$, i.e. if the arguments appropriately match the original domains as defined in (1).

Next let us introduce for an arbitrary sequence $\varrho = \varrho_1 \varrho_2 \ldots \varrho_{n-1}$, with $\varrho_i \in \big\{\mathcal{L}, \mathcal{R}\big\}$ the ϱ-forward-iterate

$$\big[f_{\varrho}\big] = \big[f_{\varrho_1 \varrho_2 \ldots \varrho_{n-1}}\big] = \big[f_{\varrho_{n-1}}\big] \circ \ldots \circ \big[f_{\varrho_1}\big] \tag{42}$$

and its inverse

$$\big[f_{\varrho}^{-1}\big] = \big[f_{\varrho_1 \varrho_2 \ldots \varrho_{n-1}}^{-1}\big] = \big[f_{\varrho_1}^{-1}\big] \circ \ldots \circ \big[f_{\varrho_{n-1}}^{-1}\big]. \tag{43}$$

Now recall that a necessary and sufficient condition for the existence of a stable period-n orbit[5] corresponding to the sequence $\varrho = \varrho_1 \varrho_2 \ldots \varrho_{n-1}$ is

$$x_0 = f_{\varrho}\big(f_{\mathcal{C}}(x_0)\big) = f_{\varrho_{n-1}} \circ \ldots \circ f_{\varrho_1} \circ f_{\mathcal{C}}(x_0), \tag{44}$$

[5]Without loss of generality we take $x_0 \in I_{\mathcal{C}}$, according to the arguments in Sec. 3.

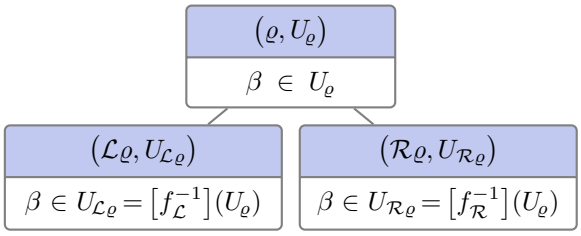

Figure 9: The Prefix Rules determine the regions of existence for symbolic sequences, based on their preimage relationship. Eqs. (37) – (39) imply that, if a node has $U = \emptyset$, so do all its successors. Thus, the resulting tree is connected and cannot contain any "orphaned" nodes.

which is equivalent to

$$f_\varrho(\beta) \in I_{\mathcal{C}}, \quad \text{and} \quad x_i \in I_{\varrho_i} \quad i = 1, \ldots, n-1. \tag{45}$$

Using the above defined interval functions (33) – (35) and (37) – (39), this condition can simply be written as

$$\beta \in \left[f_\varrho^{-1}\right](I_{\mathcal{C}})\,, \tag{46}$$

which also meets the latter conditions due to the domain constraints mentioned earlier. Especially, if any of the conditions (45) is not fulfilled, we immediately get $\left[f_\varrho^{-1}\right](I_{\mathcal{C}}) = \emptyset$.

Also it can be easily seen that $\left[f_{\mathcal{L}/\mathcal{R}}^{-1}\right](\emptyset) = \emptyset$. So if the calculation of any periodicity region by Eq. (46) is carried out iteratively, as given by Eq. (43), this calculation can be aborted with $\beta \in \emptyset$ as soon as a calculation step yields the empty set. This gives us the following procedure for determining all existing stable periodic orbits *and* existence regions thereof for any particular α, denoted as the *Prefix Rules*:

P1 Start by defining the root node $\left(\varepsilon, I_{\mathcal{C}}\right)$, where ε is the sequence and $I_{\mathcal{C}}$ the existence region.

P2 For each node, calculate $U_{\mathcal{L}\varrho} = \left[f_{\mathcal{L}}^{-1}\right](U_\varrho)$. If $U_{\mathcal{L}\varrho} \neq \emptyset$, add $\left(\mathcal{L}\varrho, U_{\mathcal{L}\varrho}\right)$ as the left child.

P3 For each node, calculate $U_{\mathcal{R}\varrho} = \left[f_{\mathcal{R}}^{-1}\right](U_\varrho)$. If $U_{\mathcal{R}\varrho} \neq \emptyset$, add $\left(\mathcal{R}\varrho, U_{\mathcal{R}\varrho}\right)$ as the right child.

These rules are also illustrated in Fig. 9. The resulting tree is connected and contains only those sequences which actually exist, as shown in Fig. 8b.

4.3. Interpretation of the results

The rules described so far allow us to construct for each particular value of α the set of all sequences corresponding to stable orbits forming the bifurcation scenario at this parameter value. For example, let us consider the situation for $\alpha = 0.6$ shown in Fig. 2a. In this case the root note ε of the tree generated with the Prefix Rules has two children, $\mathcal{R}$ and $\mathcal{L}$. The $\mathcal{R}$-node doesn't have any children, the $\mathcal{L}$-node in turn has two children, $\mathcal{RL}$ and $\mathcal{LL}$. The generation process continues in the way that the nodes with sequences containing an $\mathcal{R}$ don't have children and the other nodes $\mathcal{L}^n$ always have two children. The resulting tree is shown in Fig. 11a. Therefore, the set of sequences which correspond to orbits forming the scenario shown in Fig. 2a is given by

$$L_a \equiv L_0 := \left\{\mathcal{R}^j\mathcal{L}^n \mid n \geq 0,\, j = 0{,}1\right\}. \tag{47}$$

As one can see, for $j = 0$ we have the sequences $\mathcal{L}^n \in L_0$. The corresponding orbits are located completely in the channel between the function $f_{\mathcal{L}}$ and the principal diagonal and form the left half of the bifurcation scenario shown in Fig. 2a. The right half of this scenario is formed by the orbits corresponding to sequences $\mathcal{RL}^n \in L_0$ with $j = 1$. (One can see immediately that the ordering of the sequences in this tree is different from the ordering of the corresponding orbits in parameter space.) These orbits are also trapped in the channel but perform one additional iteration step in the right partition.

For increasing α, more and more nodes in the tree have children, so that for example for the bifurcation scenario shown in Fig. 2b at $\alpha = 0.75$ we obtain the tree shown in Fig. 11b. The set of sequences forming this tree is

$$L_b = L_0 \cup L_1 \quad \text{with} \quad L_1 = \left\{\mathcal{R}^j\mathcal{L}^n\mathcal{R}^m \mid m > 0, n \geq 0,\, j = 0{,}1\right\}. \tag{48}$$

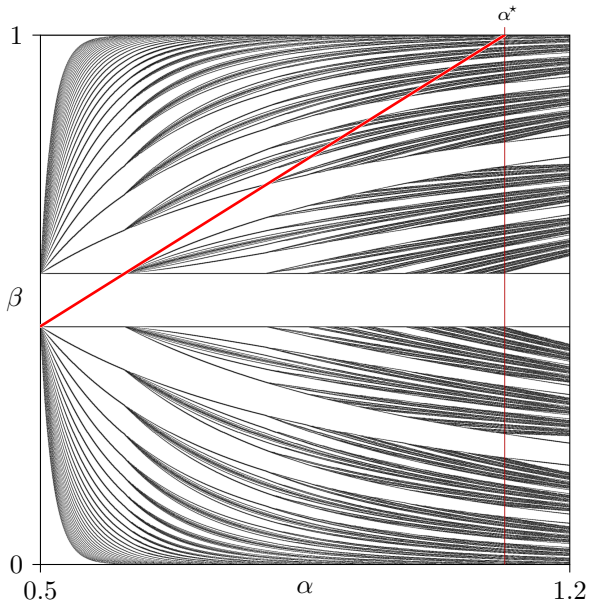

Figure 10: The thick diagonal line corresponds to the condition $\beta = (1-\gamma)\alpha$, for which (1) reduces to the *flat top tent map*. On this line, the system displays the U-sequence sequence, as introduced in [12].

Therefore, in the scenario shown in Fig. 2b all orbits that already existed in Fig. 2a are still present, but in between there are orbits corresponding to sequences from the set L_1. *Additionally* to the steps in the channel on the left partition, these orbits also perform a number of rotations in the swirl around the unstable fixed point $x_{\mathcal{R}}$ in the right partition, which is reflected by the suffix $\mathcal{R}^m$.

For α further increasing, the set of existing sequences becomes more and more complicated. So, for the scenario shown in Fig. 2c for $\alpha = 0.85$, we obtain the set

$$L_c = L_0 \cup L_1 \cup L_2 \quad \text{with} \quad L_2 = \left\{ \mathcal{R}^j \mathcal{L}^n \mathcal{R}^m (\mathcal{L}\mathcal{R})^k \mid n, m \geq 0,\, k > 0,\, j = 0{,}1 \right\}. \tag{49}$$

As one can see, the orbits corresponding to sequences from the set L_2 (which represent the extension of the scenario shown in Fig. 2c compared with the scenario shown in Fig. 2b) perform — additionally to the steps in the channel and the swirl — a number of steps jumping between the left and the right partition, as reflected by the suffix $(\mathcal{L}\mathcal{R})^k$.

The set of the sequences existing at $\alpha = 0.9$ is too complicated to be presented here. Note that the corresponding tree is shown in Fig. 8.

4.4. Unstable Orbits and Milnor Attractors

Recall that at $\alpha = \alpha^\star$ and $\beta \in M$ we observed also an infinite set of Milnor attractors (see Theorem 5).

For decreasing α the number of these attractors decreases. To give an example, Fig. 12 shows some of the curves in the (α, β)-plane where the unstable fixed point $x_{\mathcal{R}}$ in the right partition represents a Milnor attractor. These curves are defined by the conditions

$$f^k(\beta) = x_{\mathcal{R}} \equiv \frac{2\alpha}{2\alpha + 1} \quad \text{with} \quad k \geq 1 \tag{50}$$

This condition means that a typical initial value $x_0 \in \widetilde{S}$ after reaching the middle partition $I_{\mathcal{C}}$ is mapped either directly (for $k = 1$) or after some number of steps (for $k > 1$) to $x_{\mathcal{R}}$. As one can see, these curves represent the accumulation curves of the nested period incrementing cascades (for examples, of *all* nested cascades in the scenario shown in Fig. 2b). Of course, not only the unstable fixed point $x_{\mathcal{R}}$ but also other unstable periodic orbits can represent Milnor attractors as well and the corresponding parameter values can

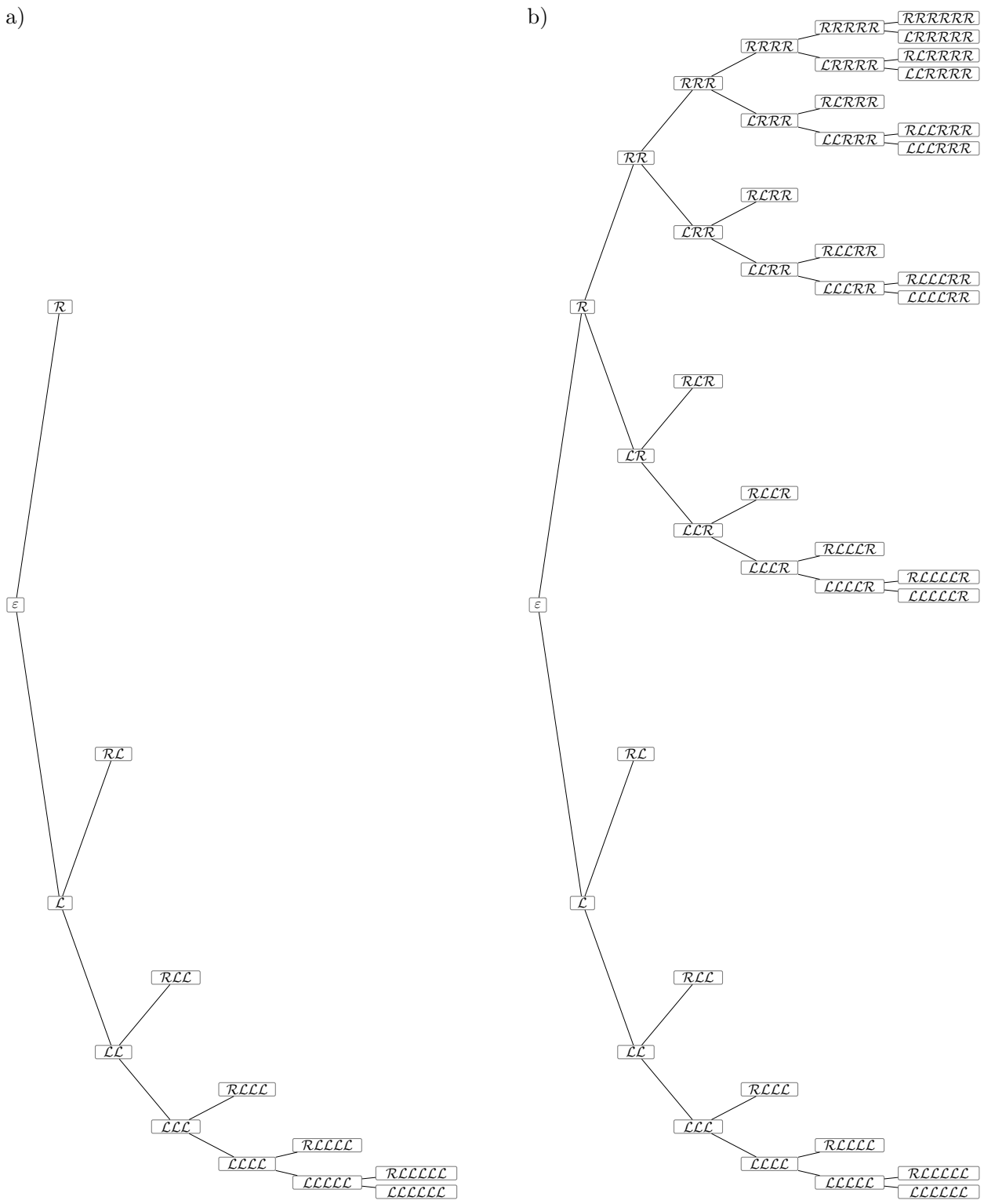

Figure 11: The symbolic sequences up to period 7, arranged according to the Prefix Rules. a) For $\alpha = 0.6$ these are the sequences belonging to the simplest scenario, the bifurcation diagram of which is shown in Fig. 2a. b) For $\alpha = 0.75$ these are the sequences existing just after the first increase in complexity at α_1, the bifurcation diagram of which is shown in Fig. 2b.

be calculated similarly. However, a detailed investigation of the unstable orbits and Milnor attractors is beyond the scope of this work, for details we refer to [18].

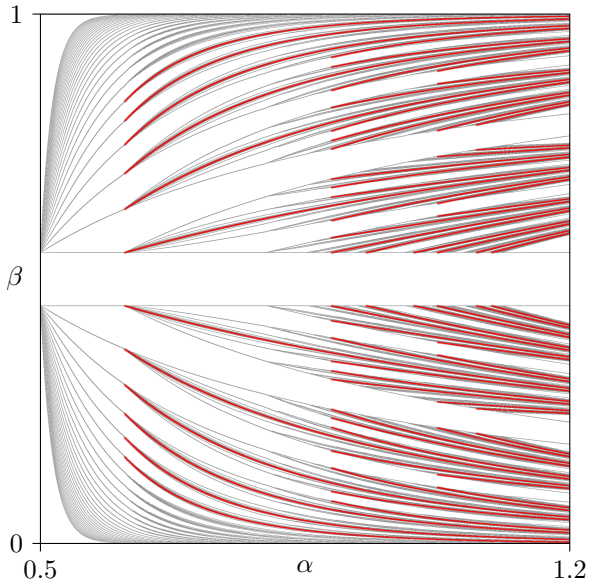

Figure 12: The red curves show the parameters fulfilling the condition (50) with $k = 1, \ldots, 7$. For these parameter values the unstable fixed point $x_{\mathcal{R}}$ is a MILNOR attractor.

5. Embedded Systems

We have derived quite a detailed description of the stable periodic dynamics of the discontinuous flat top tent map up to here. In the next step, we will investigate of which use these results can be when studying other piecewise-linear maps defined on three partitions. Recall that (1) may be considered as an extension of the flat top tent map by the parameter β. Therefore, this system is directly embedded in the parameter plane (α, β) and will be investigated first. Afterwards, another system, the truncated tent map, will be considered. It also turns out that the results obtained so far are useful for understanding of the dynamics of this system.

5.1. The Flat Top Tent Map

The logistic map is probably one of the most thoroughly investigated systems. In 1973, the authors of [12] presented a set of rules, by which the symbolic sequences of the logistic map can be generated in the order of their occurrence in parameter space. This order of symbolic sequences is thereafter known as the *U-sequence*. Independently, this structure was also described by Gumowski and Mira in [19] where it was called the box-within-a-box structure. However, as mentioned already in [12], the conditions which a map has to satisfy to display the U-sequence are fulfilled not only by the logistic map but by a broader family of unimodal maps also including the flat top tent map (which is also known as the *flat-topped tent* or *trapezoidal* map). Nevertheless, let us check whether the results we obtained for the discontinuous flat top tent map may also be useful when dealing with the original flat top tent map.

Recall that we constructed the map (1) as a discontinuous extension of the flat top tent map. Hence, the condition

$$f_{\mathcal{L}}\left(\tfrac{1-\gamma}{2}\right) = f_{\mathcal{R}}\left(\tfrac{1+\gamma}{2}\right) = f_{\mathcal{C}}(x) \tag{51}$$

leads the map (1) to be continuous, that means identical with the usual flat top tent map. As one can easily see, Eq. (51) implies

$$\beta = \alpha(1-\gamma). \tag{52}$$

This condition represents a straight line in the (α, β)-plane marked in Fig. 10. On this line, the system can be described with just one parameter[6], as which we choose α. In this case, the system is identical with the flat top tent map and thus also displays the U-sequence.

In Sec. 4.2 we considered existence regions of stable periodic orbits for fixed α, now we have to study the case for varying α. This leads clearly to a qualitative difference, because the completeness of the binary tree of symbolic sequences generated by the Prefix Rules depends on α. By inserting (52) into (46) we get

$$\alpha(1-\gamma) \in \left[f_\varrho^{-1}\right](I_\mathcal{C})\,, \tag{53}$$

where not only the left hand site but also the right hand side depends on α. The condition above is equivalent to

$$f_\varrho\big(\alpha(1-\gamma)\big) \in I_\mathcal{C}, \tag{54}$$

whereby it must be additionally guaranteed that the argument $\alpha(1-\gamma)$ is located in the domain of f_ϱ, which can be expressed as

$$\alpha \in \frac{1}{1-\gamma} D_\varrho, \quad \text{with } D_\varrho = D\big(f_\varrho\big) = \left[f_\varrho^{-1}\right]\big([0,1]\big). \tag{55}$$

Luckily, it follows from Eqs. (37) – (39) that D_ϱ is a convex set. Now the left hand side of (54) depends solely on α. Practically, this term can be considered as a curve

$$\beta = f_\varrho\big(\alpha(1-\gamma)\big),\ \alpha \in \frac{1}{1-\gamma} D_\varrho \tag{56}$$

in the parameter plane. The sequence ϱ then exists if and only if α is in the interval where this curve intersects the strip $\beta \in I_\mathcal{C}$.

Recall that, using the rules presented in [12], it is possible to determine the orbits which exist between two certain orbits in the U-sequence as follows. Given two symbolic sequences ϱ_1 and ϱ_2, one determines the harmonic and the anti-harmonic extensions of both. The symbolic sequence ϱ_3 with the lowest period existing between ϱ_1 and ϱ_2 depends on the longest common prefix of these extensions. Applied recursively ad infinitum, this approach allows to determine all orbits forming the U-sequence in a constructive manner. Note that this procedure yields the ordering of these orbits with respect to the associated parameter values, but not the exact parameter ranges for which the orbits exist.

By contrast to this approach, the conditions (54) and (55) allow us to calculate these parameter ranges directly for all stable orbits of the flat top tent map in a non-recursive manner, i.e. without prior knowledge of any other orbits of the U-sequence. Consistently, for the orbits which do not belong to the U-sequence the calculation produces an empty set.

5.2. The Truncated Tent Map

It was shown for example in [20, 21] that one of the generic situations occurring when dealing with impact oscillators can be described by maps defined on two partitions where the system function on one side of the boundary is linear and on the other side it contains linear and square-root terms. The behavior of such maps is quite complicated (see [22] for some kind of overview) and is still not understood completely. Therefore, as a very first preliminary step, we introduced in [23] the following piecewise-linear map which we denote as the truncated tent map

$$g(x) = \begin{cases} c & \text{if} \quad x < 0 \\ 2(a-c)x + c & \text{if} \quad 0 \le x \le \frac{1}{2} \\ 2a(1-x) & \text{if} \quad x > \frac{1}{2}, \end{cases} \tag{57}$$

where $c \in [0,1]$ and $a > 1$, as depicted in Fig. 13. Also shown in this figure are four partitions associated with the symbols $\mathcal{L}$, $\mathcal{M}$, $\mathcal{E}$ and $\mathcal{R}$.

[6] assuming as before that γ is fixed

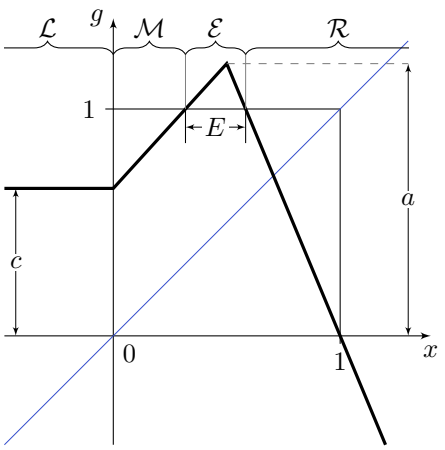

Figure 13: Truncated tent map

The period diagram in Fig. 14a of this system for c decreasing in $[0,1]$, shows a structure similar to that of the flat top tent map. For example, we can identify the first consecutive periods as 4, 8, 16 and 32, whereas already the latter exists in a very small parameter range and therefore is very hard to detect numerically. However, it turns out that the bifurcation structure produced by the truncated tent map can be efficiently investigated within the framework developed so far for the discontinuous flat top tent map.

Remarkably, the dynamics of the truncated tent map is "almost restricted" to the interval $[0,1]$, which is meant to be understood in the following way:

- Every point $x_n < 0$ gets mapped to $x_{n+1} = c$, and therefore reaches the interval $[0,1]$ in *one* iteration step.
- Every point $x_n > 1$ gets mapped to $x_{n+1} < 0$, and therefore reaches the interval $[0,1]$ in *two* iteration steps.
- Within the interval $[0,1]$, every point $x_n \in E$,

$$E = \{x \mid g(x) > 1\} = \left(\tfrac{1-c}{2(a-c)}\ ,\ \tfrac{2a-1}{2a}\right), \tag{58}$$

gets mapped to the interval $[1,a]$, and therefore *returns* to the interval $[0,1]$ in *three* iteration steps. To summarize, for every point $x_n \in E$ we obtain $x_{n+3} = c$, that means any orbit starting in E is completely predetermined after three iteration steps, regardless of the actual values of $x_{n+1} > 1$ and $x_{n+2} < 0$. In any case the symbolic representation for these three steps is $\mathcal{ERL}$. For this reason, a new map can be constructed by introducing a 'shortcut', such that every point $x \in E$ gets mapped to c in one rather than three iteration steps:

$$g'(x) = \begin{cases} 2(a-c)x + c & \text{if} \quad x \le \frac{1-c}{2(a-c)} \\ c & \text{if} \quad x \in E \\ 2a(1-x) & \text{if} \quad x \ge \frac{2a-1}{2a}. \end{cases} \tag{59}$$

The transition from the original map (57) to the map (59) is illustrated in Fig. 15. Note that any n-periodic orbit in this system, which enters the partition E, corresponds to a period $n+2$ orbit of the truncated tent map.

As can be seen in Fig. 15, the map (59) is already similar to map (1), as it is defined on three partitions of $[0,1]$ and is constant in the middle partition. However, there is a difference between the two systems, as the map (59) can still exhibit *stable* orbits of the form $\mathcal{M}^n\mathcal{R}$, which exist outside of the horizontal partition E. This difference is due to the relationship of (59) with the skew tent map [24, 25]. Recall that, in the case of the discontinuous flat top tent map, orbits that don't enter the middle partition are always unstable. In the following we consider the parameter range where such orbits are unstable in both systems. It can be

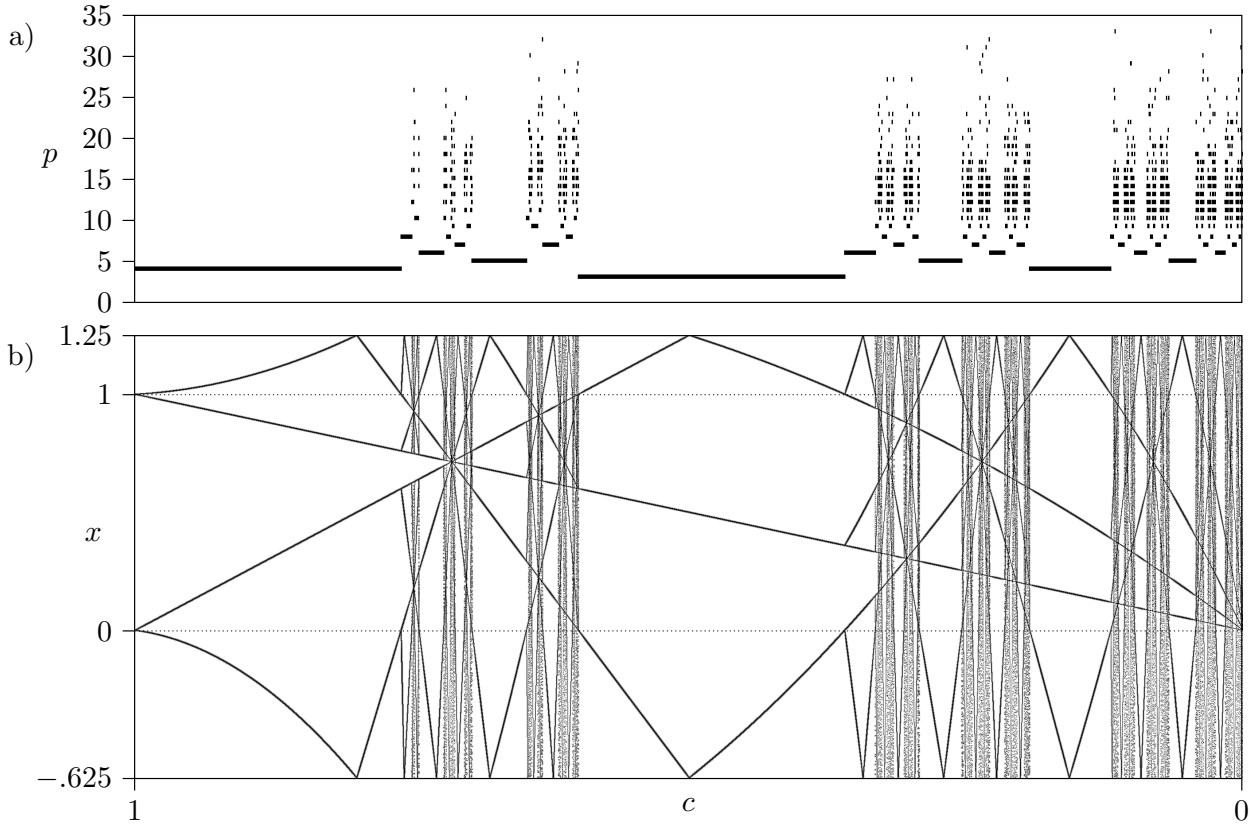

Figure 14: Period and bifurcation diagram of the truncated tent map at $a = 1.25$ for decreasing c.

shown straightforward that a sufficient condition for this requirement is

$$a > \frac{1+\sqrt{2}}{2}. \tag{60}$$

Let us now recall the most obvious difference between the map (1) and the map (57). Indeed, the former of these systems is discontinuous, whereas the latter is continuous. Although the transformed system is already discontinuous, this difference is still reflected in the fact that the functions in the left and in the middle partitions are coupled via the parameter c and hence not independent from each other. To avoid this coupling let us introduce an additional parameter $b \in [0, 1]$, which makes the value in the middle partition independent of c. The extended map now reads

$$h(x) = \begin{cases} 2(a-c)x + c & \text{if} \quad x \leq \frac{1-c}{2(a-c)} \\ b & \text{if} \quad x \in E \\ 2a(1-x) & \text{if} \quad x \geq \frac{2a-1}{2a}. \end{cases} \tag{61}$$

In the special case $b = c$, this map is identical to (59) and therefore equivalent to the truncated tent map. This condition corresponds to the diagonal line marked in the 2D bifurcation diagram in Fig. 16 on the right hand side. Furthermore, in the special case $c = 0$, the map (61) is identical to the map (1) with $\alpha = \alpha^\star$, $\beta = b$ and

$$\gamma = \frac{a-1}{a}. \tag{62}$$

In accordance with the latter condition, a is chosen to be fixed in the following. With this choice, the right

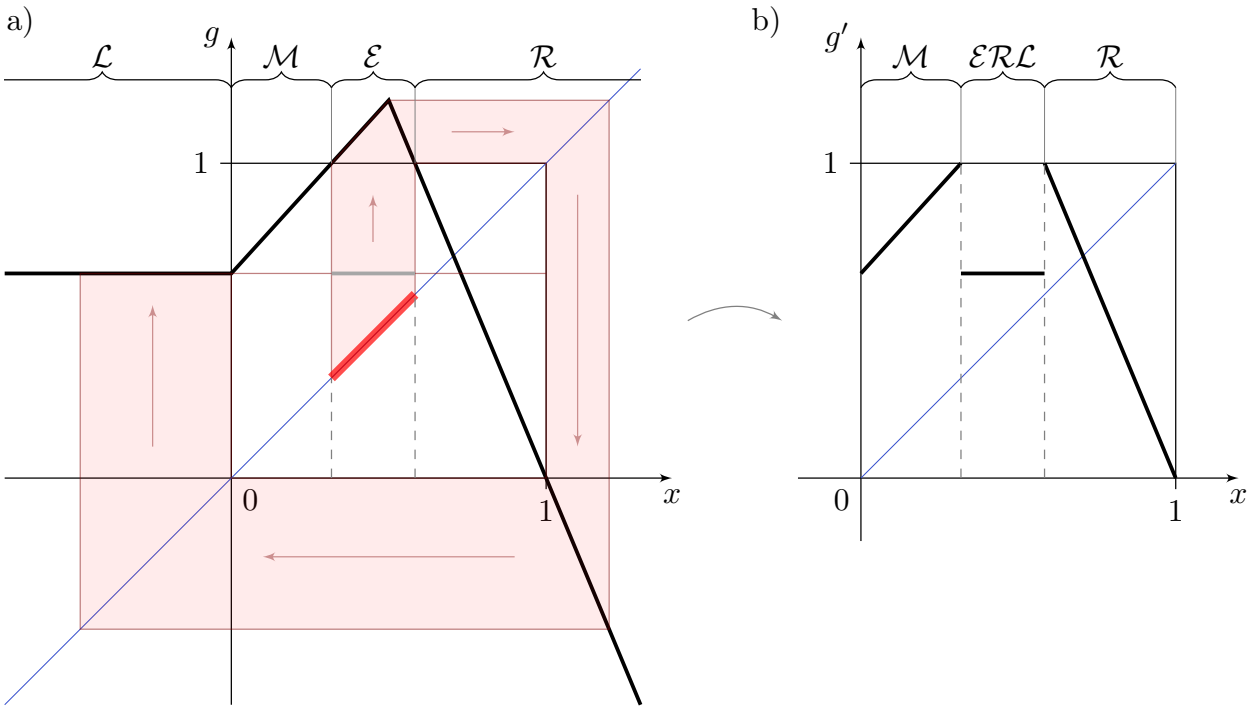

Figure 15: As one can see in a), for map (57) the third image of the interval $E = \{x \mid f(x) > 1\}$ is $f^3(E) = c$. Therefore, the map (57) can be transformed into an equivalent one (given by Eq. (59) and shown in b)) by introducing a shortcut.

boundary x_r of the middle partition

$$x_r = \frac{2a-1}{2a} = \frac{1+\gamma}{2} \tag{63}$$

is equal in both these maps for arbitrary c and α and does not depend on any other parameters. Also, both maps possess a global maximum at x_r.

For (61) the maximal value of the system function is constantly $h(x_r) = 1$, regardless of the parameters. Therefore, for any choice of parameter values the map has the invariant absorbing interval given by

$$A_h = \big[h^2(x_r), h(x_r)\big] = [0, 1]. \tag{64}$$

This is, of course, the state space where the dynamics of the (transformed) truncated tent map h takes place, as well as the set of admissible values for the parameter b. Finally, we note that if b is set to the *image* of the left endpoint of A_h, $h^3(x_r) = c$, the system is equivalent to the truncated tent map.

Now, if we consider the maximal value of the function f in Eq. (1), we see that the value varies with α, namely $f(x_r) = \alpha(1-\gamma)$. This also implies that the absorbing interval[7] in this case is parameter-dependent:

$$A_f = \big[f^2(x_r), f(x_r)\big] = \Big[2\alpha - 2\alpha^2(1-\gamma),\ \alpha(1-\gamma)\Big] \tag{65}$$

The endpoints of this interval for varying α are shown as the upper and lower boundaries of the region R in Fig. 16. The left and right boundaries of R are given by the condition that the lower endpoint of the absorbing interval should lie in the left partition, which translates to

$$\alpha \in \left[\frac{1+\sqrt{\gamma(2-\gamma)}}{2(1-\gamma)},\ \alpha^\star\right]. \tag{66}$$

[7]Here we calculate the absorbing interval only with respect to the left and right partition, assuming that β is chosen from within this interval for all subsequent argumentation.

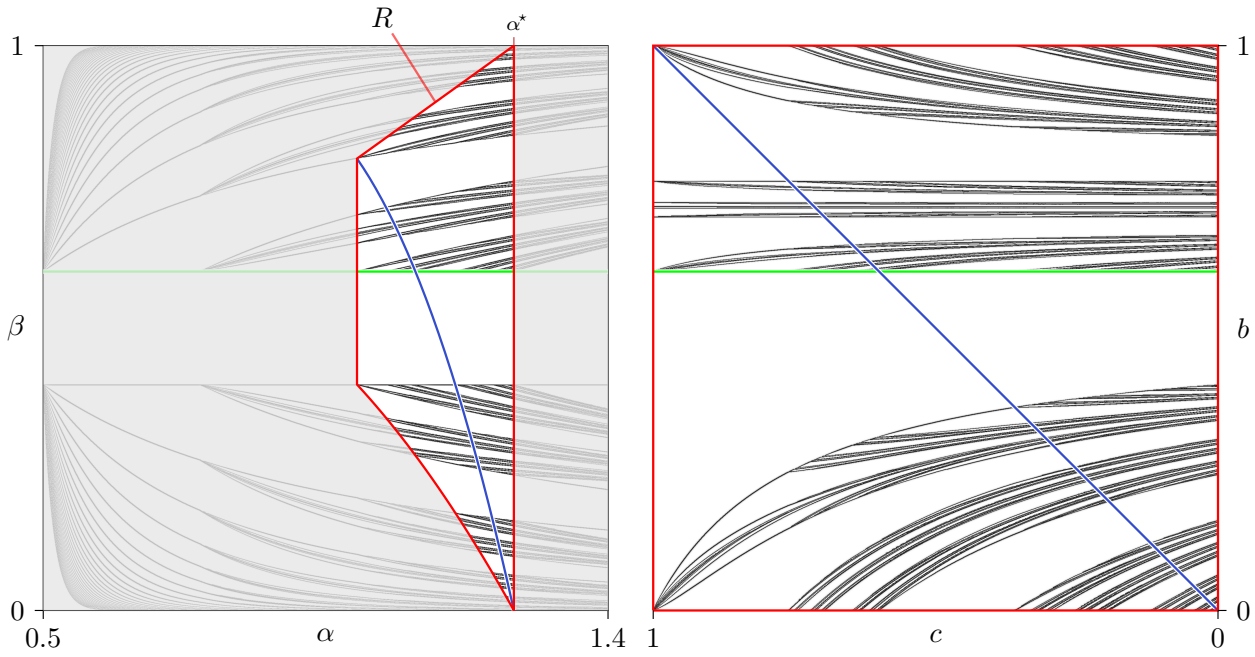

Figure 16: The mapped parameter plane of the truncated tent map. On the right is the bifurcation structure of the original map (61) for $a = 1.25$ in the (c, b)-plane. On the left is the region R in the bifurcation structure of the discontinuous flat top tent map for $\gamma = 0.2$, displaying the same topological structure.

In particular, the left boundary of R, where the intersection of A_f and $I_{\mathcal{L}}$ shrinks to a point, corresponds to the situation $c = 1$ in (61), where the $\mathcal{M}$-partition vanishes.

The diagonal curve traversing R in the figure corresponds to the case where β is set to the image of the left endpoint of A_f, i.e. the equivalent of the case $b = c$ in (61) which is in turn equivalent to the truncated tent map. This curve is given by

$$\beta = f^3(x_r) = 4\alpha^2 - 4\alpha^3(1-\gamma). \tag{67}$$

Now we can determine the bifurcation scenario occurring along this curve. We already know that on the curve $\beta = \beta' = f(x_r) = \alpha(1-\gamma)$, the discontinuous flat top tent map displays the U-sequence, cf. (52). To arrive at condition (67), however, we have to consider this curve twice iterated, that is $\beta = f^2(\beta')$. Luckily, we are able to infer the relationship of this case to the U-sequence from the following

Lemma 4. *Assume conditions (5) and (6). If for $\beta = \beta'$ map (1) has a stable orbit of period $n > 1$ with the $\mathcal{C}$-reduced sequence*

$$\varrho' = \varrho_1 \varrho_2 \dots \varrho_{n-1}, \tag{68}$$

then for $\beta = \beta'' = f(\beta')$ there is a stable orbit of period $n-1$ with the $\mathcal{C}$-reduced sequence

$$\varrho'' = \varrho_2 \dots \varrho_{n-1}. \tag{69}$$

In particular, for $n = 2$ we have $\varrho' = \varrho_1$ and $\varrho'' = \varepsilon$. Lemma 4 follows as the converse of Lemma 3. This means that on the curve given by (67) the orbits of the discontinuous flat top tent map have the same $\mathcal{C}$-reduced sequences as for the flat top tent map (those of the U-sequence), but reduced by two letters at the beginning. For example, in the interval $\alpha \in I_{\mathcal{RLR}}$, where the flat top tent map has the period-4 orbit with $\varrho = \mathcal{RLR}$, there is a period-2 orbit with $\varrho = \mathcal{R}$ for (67).

5.3. Modified U-sequences

As shown above, the discontinuous flat top tent map displays the U-sequence for parameters varied along the line given by $\beta = \alpha(1-\gamma)$. Furthermore, we have also seen that for parameters varied along the

curve $\beta = f^2\big(\alpha(1-\gamma)\big)$, map (1) displays a scenario similar to the U-sequence, but where the period of each involved orbit is reduced by two. This observation can also be further generalized. To this end let us consider the forward and backward iterations of the curve $u(\alpha)$ in parameter space, defined by

$$\beta = u(\alpha) = \alpha(1-\gamma), \quad \alpha \in \left[\tfrac{1}{2}, \alpha^\star\right], \tag{70}$$

which are given by

$$\beta = f^k\big(u(\alpha)\big) \tag{71}$$

$$\text{and} \qquad \beta = f_\sigma^{-1}\big(u(\alpha)\big),\ \sigma \in \{\mathcal{L},\mathcal{R}\}^k,\ k \geq 1. \tag{72}$$

The symbolic sequences corresponding to the orbits occurring along the curve given by (71) can be determined as follows: from each $\mathcal{C}$-reduced sequence of length $n-1$ occurring in the U-sequence, remove the prefix of length $\min\{k,(n-1)\}$. This follows from Lemma 4, with the restriction that an orbit of period 1 cannot be further reduced. This procedure generates bifurcation scenarios which display the U-sequence with a negative period-k offset, and accordingly a cutoff at period k. To give an example, for $\beta = f^3\big(u(\alpha)\big)$, the scenario begins with the periods 1, 5, 13, 29, 61, ...

For the curves in parameter space given by Eq. (72) the procedure is similar: to each $\mathcal{C}$-reduced sequence occurring in the U-sequence, add the prefix σ of length k. This follows from Lemma 3. The resulting bifurcation scenarios display the U-sequence with a positive period-k offset. Here it has to be taken into account, that the α-domain of the parameter curve will be only a subset of $\left[\frac{1}{2}, \alpha^\star\right]$, in general. This is due to the fact that the domain of $f^{-1}_{\mathcal{L}/\mathcal{R}}(\beta)$ is restricted to $\beta \in \big[0, \alpha(1-\gamma)\big]$.

6. Summary and Outlook

In this work we considered the discontinuous extension of the well-known flat top tent map (called *discontinuous flat top tent map*) and investigated a new bifurcation scenario formed by stable periodic orbits of this map. This scenario, denoted as the *nested period incrementing* structure, was first investigated at a particular parameter value $\alpha = \alpha^\star$, where it is fully developed. Then it has been generalized to other values of α, where it occurs in a truncated form. In both cases, a binary tree arrangement reveals several simple mechanisms, which determine the existence and ordering of periodic orbits, according to their respective symbolic sequences. Furthermore, two examples have shown that the results for the discontinuous flat top tent map can also be applied for the investigation of other three-partition maps with a constant interval, and how the famous *U-sequence* is embedded within the nested period incrementing structure.

Acknowledgment

The authors thank Prof. Laura Gardini from the University of Urbino, Italy, for valuable discussions which significantly improved this work.

References

[1] K. Myneni, T. A. Barr, N. J. Corron, S. D. Pethel, New method for the control of fast chaotic oscillations, Phys. Rev. Lett. 83 (1999) 2175.

[2] C. Wagner, R. Stoop, Optimized chaos control with simple limiters, Phys. Rev. E 63 (2000) 017201.

[3] C. Wagner, R. Stoop, Renormalization Approach to Optimal Limiter Control in 1-D Chaotic Systems, Journal of Statistical Physics 106 (1/2) (2002) 97–107.

[4] C. Wagner, R. Stoop, Scaling Properties of Simple Limiter Control, Physical Review Letters 90 (15) (2003) 154101.

[5] F. Hilker, F. H. Westerhoff, Paradox of simple limiter control, Physical Review E 73 (5) (2006) 052901(3). doi:10.1103/PhysRevE.73.052901.

[6] N. Corron, S. Pethel, B. Hopper, Controlling Chaos with Simple Limiters, Phys. Rev. Lett 84 (17) (2000) 3835.

[7] L. Glass, W. Zeng, Bifurcations in Flat-Topped Maps and the Control of Cardiac Chaos, International Journal of Bifurcation and Chaos 4 (4) (1994) 1061–1067.

[8] A. Garfinkel, M. Spano, W. Ditto, J. Weiss, Controlling cardiac chaos, Science 257 (1992) 1230.

[9] A. Amann, K. Peters, U. Parlitz, A. Wacker, E. Schll, Hybrid Model for Chaotic Front Dynamics: From Semiconductors to Water Tanks, Physical Review Letters 91 (6) (2003) 066601.
[10] T. Kabe, S. Parui, H. Torikai, S. Banerjee, T. Saito, Analysis of Piecewise Constant Models of Current Mode Controlled DC–DC Converters, IEICI Trans. Fundamentals E90-A (2) (2007) 448.
[11] Y. Matsuoka, T. Saito, Rotation Map with a Controlling Segment and Its Application to A/D Converters, IEICI Trans. Fundamentals E91-A (7) (2008) 1725–1732.
[12] N. Metropolis, M. L. Stein, P. R. Stein, On Finite Limit Sets for Transformations on the Unit Interval, Journal of Combinatorial Theory, Series A 15 (1) (1973) 25–44.
[13] K. Zyczkowski, E. Bollt, On the entropy devils staircase in a family of gap-tent maps, Physica D 132 (1999) 392–410.
[14] I. Sushko, L. Gardini, Degenerate Bifurcations and Border Collisions in Piecewise Smooth 1D and 2D Maps, International Journal of Bifurcation and Chaos 20 (7) (2010) 2045–2070.
[15] K. T. Alligood, T. D. Sauer, J. A. Yorke, CHAOS: An Introduction to Dynamical Systems, Springer, 1996.
[16] J. Milnor, On the Concept of Attractor, Communications in Mathematical Physics 99 (1985) 177–195.
[17] L. Jaulin, M. Kieffer, O. Didrit, E. Walter, Applied Interval Analysis with Examples in Parameter and State Estimation, Robust Control and Robotics, Springer, 2001.
[18] V. Avrutin, B. Futter, L. Gardini, M. Schanz, Unstable orbits and milnor attractors in the discontinuous flat top tent map, European Series in Applied and Industrial Mathematics: Proceedings(to appear).
[19] I. Gumowski, C. Mira, Accumulation de bifurcations dans une récurrence, Comptes Rendus Acad. Sc. Paris, Série A (1975) 45–48.
[20] J. Molenaar, J. G. de Weger, W. van de Water, Mappings of grazing-impact oscillators, Nonlinearity 14 (2001) 301–321.
[21] S. Kundu, S. Banerjee, D. Giaouris, Vanishing singularity in hard impacting systems, Discrete and Continuous Dynamical Systems - Series B 16 (1) (2011) 319 – 332. doi:10.3934/dcdsb.2011.16.319.
[22] V. Avrutin, P. Dutta, M. Schanz, S. Banerjee, Influence of a square-root singularity on the behavior of piecewise smooth maps, Nonlinearity 23 (2010) 445–463. doi:10.1088/0951-7715/23/2/012.
[23] V. Avrutin, M. Schanz, B. Schenke, On a bifurcation structure mimicking period adding, Proc. R. Soc. A 467 (2129) (2011) 1503–1518. doi:10.1098/rspa.2010.0573.
[24] Y. L. Maistrenko, V. L. Maistrenko, L. O. Chua, Cycles of Chaotic Intervals in a Time–Delayed Chua's Circuit, Int. J. Bifurcation Chaos 3 (1993) 1557–1572.
[25] Y. L. Maistrenko, V. L. Maistrenko, S. I. Vikul, L. O. Chua, Bifurcations of Attracting Cycles from Time–Delayed Chua's Circuit, Int. J. Bifurcation Chaos 5 (1995) 653–671.